Chapter 1
The Boar Spermatozoon

M. Dolors Briz and Anna Fàbrega

Abstract The microscopic appearance of the boar spermatozoon allows us to appreciate both its inner and outer structural complexity. Both light and electron microscopy may be used to study the structure and ultrastructure of this highly specialized cell and the way it probably works to achieve successful fertilization. Compartmentalization of the spermatozoon is a critically important feature of its structure as it enables this cell to perform the variety of tasks needed to fulfill its role. Different sperm malformations usually affect some cellular components essential for the correct development of the spermatozoon–oocyte interaction in the fertility process. Careful assessment of sperm morphology may sometimes indicate the possible cause of sperm quality and fertility decrease. Moreover, regional specialization of the plasma membrane, related to lipid/protein composition and distribution, allows the underlying cellular molecules to interact independently with their external environment, thereby enabling the efficient performance of the various tasks necessary for successful fertilization.

1.1 Introduction

The practice of artificial insemination (AI) in pigs has undergone a major expansion in the past two decades, mainly due to its greater advantages in comparison to natural mating, and the increased trend toward industrialized large porcine livestock production in contrast with small farms. AI practice only provides acceptable results in terms of fertility and prolificity when boar ejaculates exhibit excellent sperm quality. Sperm morphology is an essential criterion for the assessment of sperm fertilizing ability; thus, proper evaluation of the morphological characteristics, and especially of sperm malformations, represents a fundamental part of a routine seminal analysis of boar ejaculates (see Sect. 11.3.3).

M. D. Briz (✉) · A. Fàbrega
Biotechnology of Animal and Human Reproduction (TechnoSperm), Department of Biology, Institute of Food and Agricultural Technology, University of Girona, Campus Montilivi, 17071 Girona, Spain
e-mail: mailo.briz@udg.edu

S. Bonet et al. (eds.), *Boar Reproduction*, DOI: 10.1007/978-3-642-35049-8_1,

A careful assessment of sperm morphology may indicate, in some cases, the likely cause of sperm quality and fertility decrease (Bonet et al. 1992, 1995; Briz et al. 1996).

In livestock production, particularly in AI and in selection and multiplication centers, the presence of infertile or subfertile boars has great negative repercussions because, in principle, between 10 and 15 females can be inseminated with the ejaculate of a single male; for this reason, in these porcine production centers the study of sperm morphology of boar ejaculates becomes a routine control and, besides being a male fertility indicator, it is used as a basic parameter for the etiological diagnosis of infertility and subfertility. There is a wide range of factors capable of affecting the sperm morphology of a boar ejaculate, basically, dysfunctions of the reproductive system (testicular, epididymal, or sex gland pathologies), genetic factors (breed, congenital pathologies), environmental factors (temperature, humidity, photoperiod), and/or husbandry factors (nutrition, socialization, sperm handling, frequency of semen collection) (see Chap. 4). Sometimes, it is possible to establish a correlation between the agent responsible for infertility or subfertility and the presence of a high percentage of a specific sperm malformation. In this sense, for example, a high frequency of semen collections without resting periods often results in a fertility decrease produced by the presence of a remarkable rise in immature spermatozoa, of spermatozoa with tails bent at the annulus and of spermatozoa with coiled tails in the ejaculate (Bonet 1987, 1990; Bonet and Briz 1991b; Briz et al. 1993; Pruneda et al. 2005).

The accurate assessment of images obtained by means of light and electron microscopy allows us to appreciate the extreme structural complexity of both the surface and the inside of the boar spermatozoon (Figs. 1.1 and 1.2) (Bonet and Briz 1991a; Briz et al. 1993, 1995; Briz 1994; Bonet et al. 1994a, b, 2000, 2006). As with many other mammalian spermatozoa, the boar spermatozoon is a highly specialized cell with a characteristic surface morphology containing different cellular compartments, as clearly seen through its different ultrafine cross-sections, which can be examined in great detail under transmission electron microscopy (Fig. 1.2). At first glance, the ejaculated boar spermatozoon is a cell with a compact head, an acrosome associated with the nucleus, a well-developed mitochondrial sheath and coarse or outer dense fibers in the tail (Figs. 1.3, 1.4, 1.5, 1.6).

Different sperm malformations usually affect some of the cellular structures (acrosome, nucleus, mitochondria, axoneme, plasma membrane, etc.) (Figs. 1.7, 1.8, 1.9, 1.10, 1.11, 1.12, 1.13, 1.14, 1.15, 1.16) essential for the correct development of the spermatozoon–oocyte interaction in the fertility process (Bonet 1990; Bonet and Briz 1991b; Bonet et al. 1993); if any one of these malformations occurs in an important number of the ejaculated spermatozoa, the male is likely to be subfertile or, in the worst of cases, infertile.

The boar sperm plasma membrane, as in all other animal cell types, is a continuously limiting cell boundary that serves to maintain cell integrity, and which forms a dynamic interface between the cell and its immediate environment. Despite this, and in contrast to many other cell types, both the structure and function of the sperm plasma membrane is highly heterogeneous with different sharply

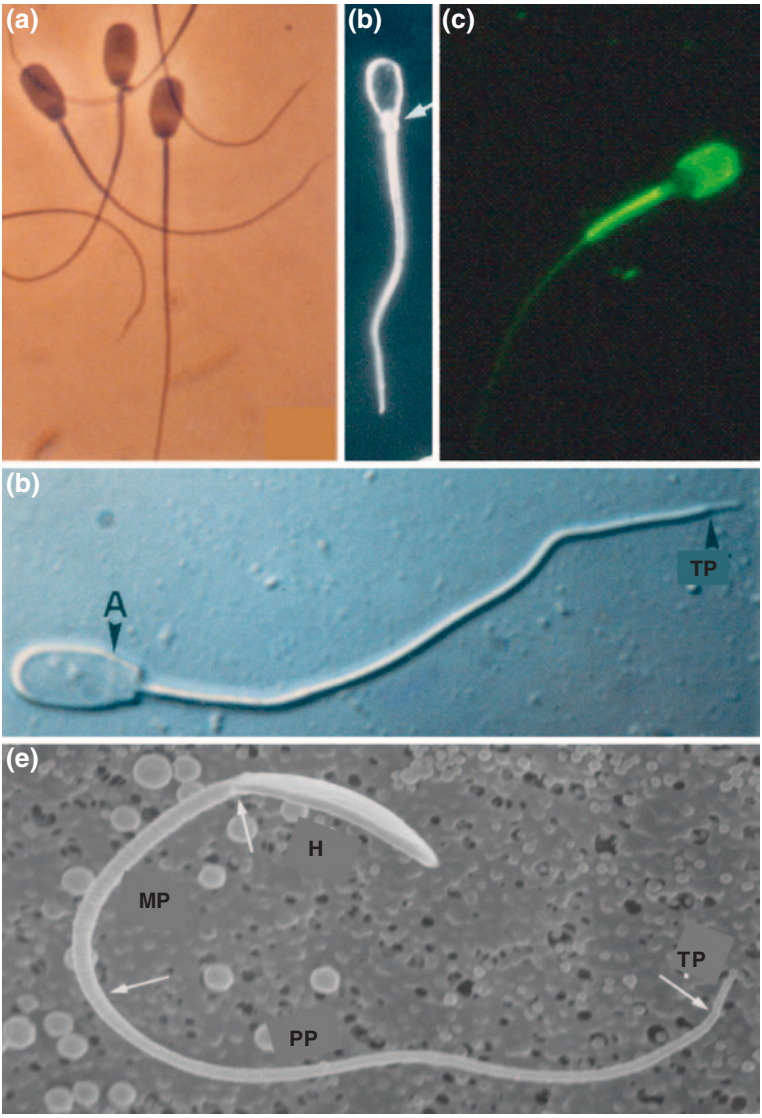

Fig. 1.1 Light (**a**–**d**) and electron (**e**) micrographs showing the general structure of the boar spermatozoon. **a** Mature spermatozoa; positive phase-contrast light microscopy (×1,400). **b** Immature spermatozoon with proximal cytoplasmic droplet (*arrow*); dark-field light microscopy (×1,000). **c** Mature spermatozoon; fluorescence light microscopy (×1,600). **d** Mature spermatozoon; *A*, acrosomal vesicle limit; terminal piece (*TP*); Nomarski interference contrast light microscopy (×2,700). **e** Side view of a mature spermatozoon (*arrows point to the boundaries between several cell regions*); head (*H*); midpiece (*MP*); principal piece (*PP*); terminal piece (*TP*); scanning electron microscopy (×5,800)

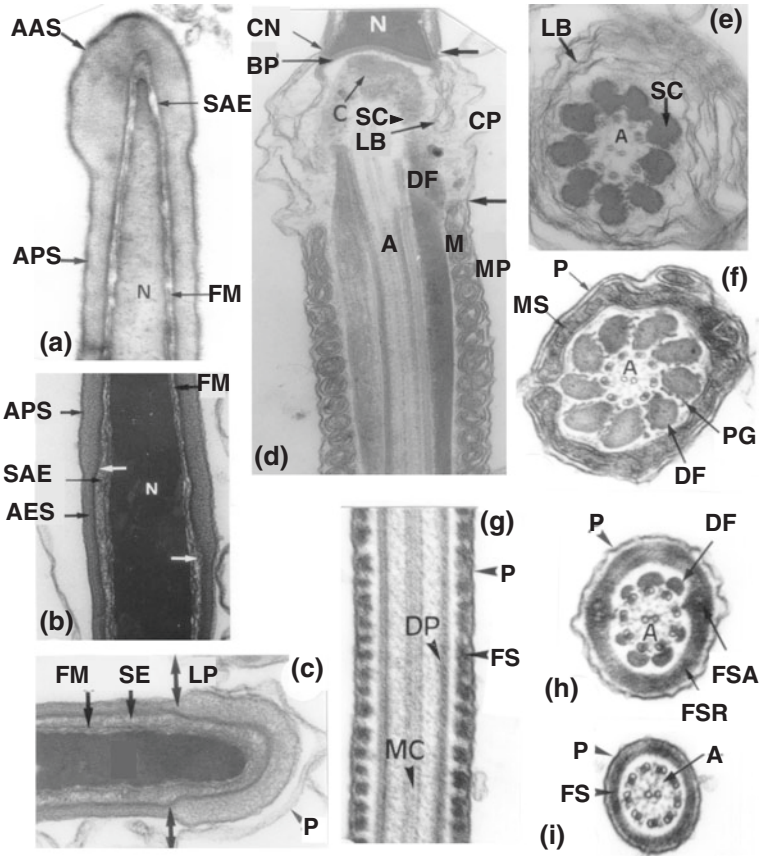

Fig. 1.2 Transmission electron micrographs showing the ultrastructure of the boar spermatozoon in its major parts: head (**a**–**c**), connecting piece (**d**–**e**) and tail (**f**–**i**). **a** Sagittal section through the apical (*AAS*) and principal (*APS*) segments of the acrosome (×80,000). **b** Sagittal section of the acrosome principal (*APS*) and equatorial (*AES*) segments (*white arrows point to the limit between these two segments*) (×80,000). **c** Cross section at the lateral protuberance (*LP*) level of the acrosome equatorial segment (*double arrows indicate the limit of the LP*) (×90,000). **d** Longitudinal section of the connecting piece (*CP*) (*arrows point to the limits of the CP*) (×70,000). **e** Cross section through the connecting piece (×85,000). **f** Cross section through the midpiece (*MP*); notice the nine peripheral microtubule doublets and the central microtubule pair of the axoneme (*A*) (×80,000). **g** Longitudinal section of the principal piece (*PP*) (×80,000). **h** Cross section through the mid-anterior region of the principal piece (×80,000). **i** Cross section through the mid-posterior region of the principal piece (×80,000). axoneme (*A*); basal plate (*BP*); capitulum (*C*); circular neckline (*CN*); dense fibers (*DF*); peripheral microtubule doublet (*DP*); perinuclear fibrous material (*FM*); fibrous sheath (*FS*); fibrous sheath axes (*FSA*); fibrous sheath ribs (*FSR*); laminar bodies (*LB*); mitochondria (*M*); central microtubule pair (*MC*); mitochondrial sheath (*MS*); nucleus (*N*); plasmalemma (*P*); peripheral granules (*PG*); subacrosomal space (*SAE*); segmented columns (*SC*)

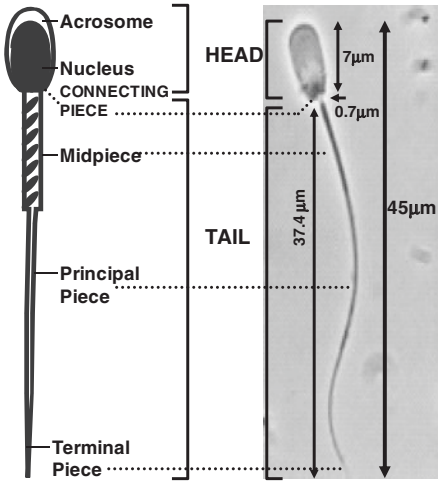

DIMENSIONS OF NORMAL MATURE BOAR SPERMATOZOA	Length (µm)	Width / Diameter (µm)
Whole spermatozoon	45.0	-
Head	7.0	3.7 (0.4[a])
Connecting piece	0.7	0.5
Tail	37.4	-
midpiece	9.0	0.7
principal piece	26.2	0.4
terminal piece	2.2	0.2

[a]Thikness

Fig. 1.3 Diagrammatic representation of the major parts of normal mature boar spermatozoa and their typical dimensions. The head contains the cell nucleus and the acrosome and the tail can be divided into three regions: the midpiece, the principal piece, and the terminal piece. Between head and tail there is a short linking segment, the connecting piece (or neck). Every part and region presents characteristic dimensions

defined membrane domains. Extensive biochemical studies have shown that the mammalian sperm surface is organized into lipid domains (with differences in membrane fluidity and lipid composition) significantly different from those in somatic cells and, that most sperm plasma membrane proteins also reveal a high degree of mosaicism (with differences in intramembranous particle distribution and membrane surface antigens and charge). This regional specialization, evidenced by biochemical and immunological parameters, reflects both the specific surface properties and the unique structure of this membrane. Moreover, membrane domains established during passage through the male reproductive tract are not fixed, but undergo reorganization during the capacitation process within the female reproductive tract (see Chap. 7). Thus, after the many modifications occurring in the testis, epididymis and oviduct, mammalian spermatozoa must be capable of fertilizing the oocyte (Thaler and Cardullo 1995; Curry and Watson 1995). The surface of boar sperm is in fact highly heterogeneous and has a molecular ordering that reflects the polar distribution of the main organelles (acrosome, nucleus, and mitochondria) and the cytoskeletal elements that lie under the surface (annulus, fibrous sheath and axoneme) (Phelps et al. 1990; Gadella et al. 1995). In this sense, different domains of the sperm surface (up to five) can be distinguished with separate functions in the fertilization process (Brewis and Gadella 2010). These various membrane domains differ in their binding affinity for lectins, thereby reflecting differences in the extent and composition of their glycocalyx (Fig. 1.17) (Fàbrega et al. 2011a, b).

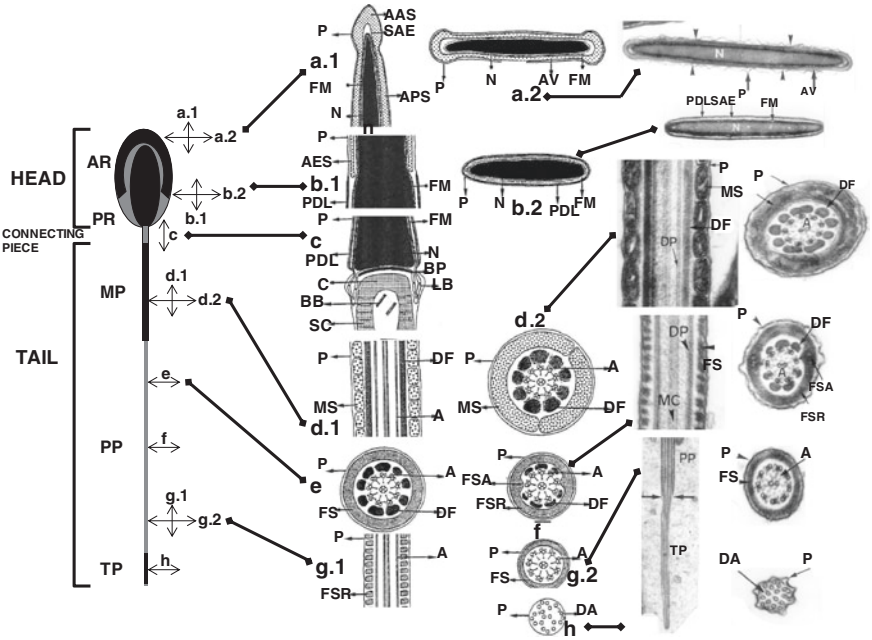

Fig. 1.4 Diagrammatic representation and micrographs of longitudinal and cross sections through the head (**a**–**b**), connecting piece (**c**) and tail (**d**–**h**) of the boar spermatozoon illustrating the main components. **a.1** Apical and principal segments of the acrosomal region (*AR*); **a.2** acrosomal region; **b.1** equatorial segment of the acrosomal and postacrosomal region (*PR*); **b.2** postacrosomal region; **c** postacrosomal region and connecting piece (or neck); **d.1** and **d.2** midpiece (*MP*); **e** proximal region of the principal piece (*PP*); **f** Intermediate region of the principal piece; **g.1** and **g.2** distal region of the principal piece; **h** terminal piece (*TP*). Axoneme (*A*); acrosomal vesicle or acrosome (*AV*); acrosome apical segment (*AAS*); acrosome equatorial segment (*AES*); acrosome principal segment (*APS*); axoneme (*A*); basal body (*BB*); basal plate (*BP*); capitulum (*C*); circular neckline (*CN*); disorganized axoneme (*DA*); dense fibers (*DF*); peripheral microtubule doublet (*DP*); perinuclear fibrous material (*FM*); fibrous sheath (*FS*); fibrous sheath axes (*FSA*); fibrous sheath ribs (*FSR*); laminar bodies (*LB*); mitochondria (*M*); central microtubule pair (*MC*); midpiece (*MP*); mitochondrial sheath (*MS*); nucleus (*N*); plasmalemma (*P*); postacrosomal dense lamina (*PDL*); peripheral granules (*PG*); subacrosomal space (*SAE*); segmented columns (*SC*)

1.2 The Ejaculated Spermatozoon

This section describes the general and detailed traits of mature boar spermatozoa present in normal ejaculates (Figs. 1.1–1.6).

1.2.1 General Structure and Function

The general structure of spermatozoa responds to their basic function, to reach and fertilize the oocyte, thereby becoming specialized for their reproductive role.

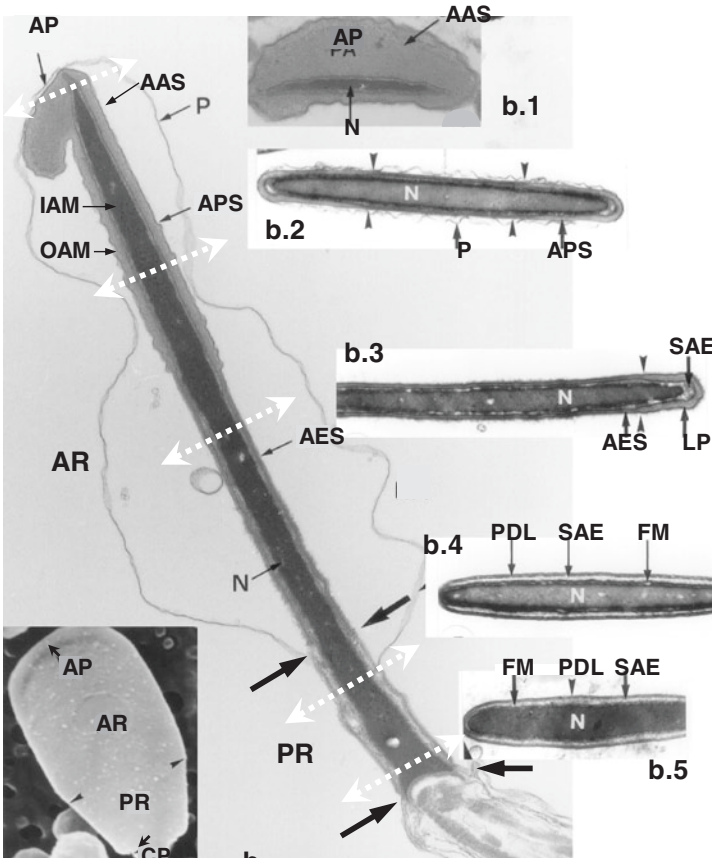

Fig. 1.5 Scanning (**a**) and transmission (**b**) electron micrographs showing the ultrastructure of the head of a mature boar spermatozoon. **a** Detail of a mature spermatozoon head; the *arrows* point to the boundaries between several spermatozoic regions: acrosomal protuberance (*AP*), acrosomal region (*AR*), postacrosomal region (*PR*) and connecting piece (*CP*). (×11,400). **b** Midsagittal section through the mature spermatozoon head; the *black thicker arrows* point to the limit between the connecting piece (*CP*), the postacrosomal region (*PR*) and the acrosomal region (*AR*). The plasmalemma (*P*) is detached from the acrosomal region and firmly adhered to the postacrosomal region (small changes in the osmolarity of the media used for the process of the seminal samples provoke this plasmolysis that, when slight, only affects the acrosomal cephalic region). Notice the following structures: acrosome apical segment (*AAS*); acrosome principal segment (*APS*); acrosome equatorial segment (*AES*); inner acrosomal membrane (*IAM*); outer acrosomal membrane (*OAM*) and nucleus (*N*) (×30,000). The *white arrows* indicate the orientation and the level of the sections depicted in figure **b.1–b.5**. **b.1** Cross section through the acrosome apical segment (*AAS*) at the level of the acrosomal protuberance (*AP*) (×31,500). **b.2** Cross section through the acrosome principal segment (*APS*) showing that the acrosome is slightly thinner in the central zones of the two faces of the head; the *arrowheads* indicate the limit of these differences in thickness of the acrosome. (×30,000). **b.3** Cross section of the acrosome equatorial segment (*AES*) showing that in this region the acrosome is thicker in the lateral zones of the head (lateral protuberance, *LP*); the *arrowheads* indicate the beginning of the lateral protuberance. Notice the subacrosomal space (*SAE*) underlying the lateral protuberance is highly developed (×30,000). **b.4** Cross section of the postacrosomal region closer to the acrosomal region and, **b.5** *closer to the connecting piece*. Notice the postacrosomal dense lamina (*PD*), the subacrosomal space (*SAE*) and the perinuclear fibrous material (*FM*) (×30,000)

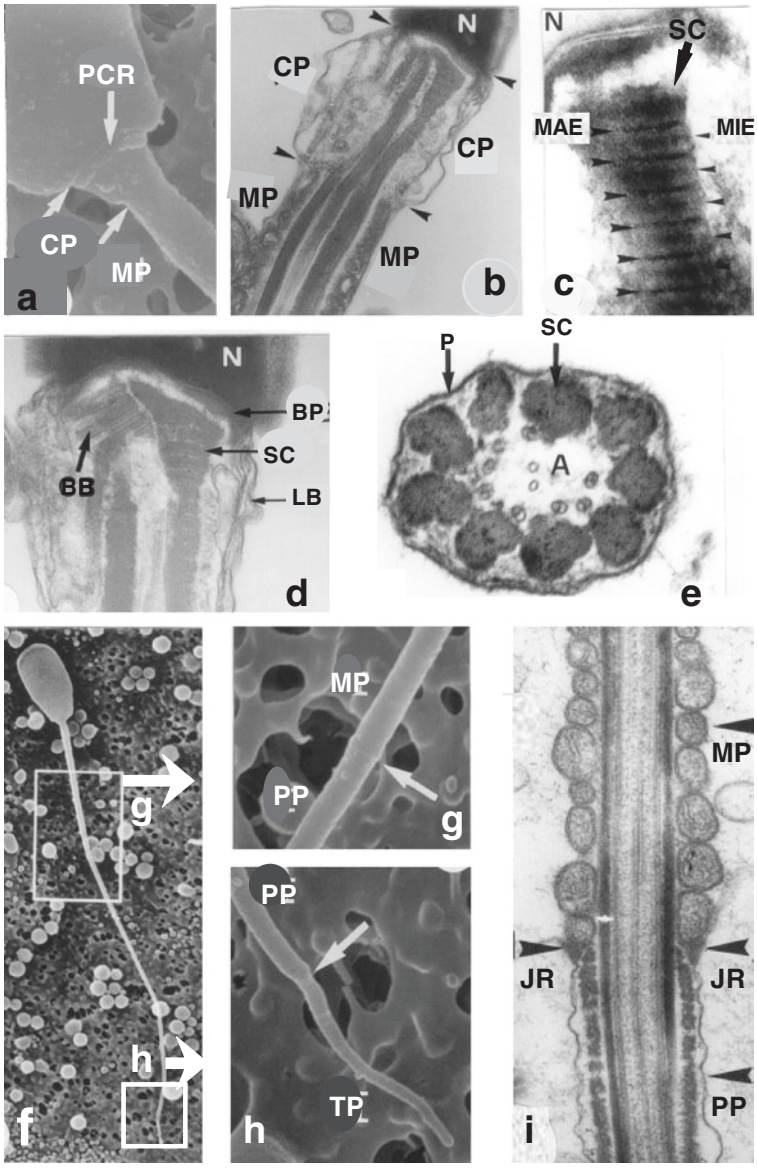

Spermatozoa are small in size and are highly mobile cells, containing the DNA that the male will contribute to the next generation and little more than the elements required to move toward the oocyte and achieve fertilization. Many details in the structure and function of spermatozoa are determined by their own genome (most of the sperm phenotype is controlled by the diploid genotype of the male), and possibly this is a component of the mechanism whereby speciation is controlled (Austin 1995). The spermatozoon has developed a highly specialized morphology

◀ **Fig. 1.6** Scanning (**a**, **f**–**h**) and transmission (**b**–**e**, **i**) electron micrographs showing the ultrastructure of the connecting piece and the tail of a mature boar spermatozoon. **a** Detail of the connecting piece (*CP*) of a mature spermatozoon; notice the postcephalic ring (*PCR*) (×10,000). **b** Longitudinal section of the connecting piece (*CP*); the *arrowheads* point to its limits (×40,000). **c** Longitudinal section through the segmented columns (*SC*); the *arrowheads* show the periodicity of the major (*MAE*) and minor striation (*MIE*) (×110,000). **d** Longitudinal section of the connecting piece; detail of the basal plate (*BP*), basal body (*BB*), segmented columns (*SC*) and laminar bodies (*LB*) (×65,000). **e** Cross section through the connecting piece at the mid-posterior region level (without laminar bodies); notice the microtubules of the axoneme (*A*) (×100,000). **f** General view of a mature spermatozoon; the framed areas are enlarged in figures **g** and **h**. **g** The arrow points to the junction of the midpiece (*MP*) and the principal piece (*PP*) of the spermatozoon tail (×14,000). **h** The *arrow points* to the limit between the tail principal (*PP*) and terminal (*TP*) pieces (×14,000). **i** Longitudinal section through the limit between the midpiece (*MP*) and the principal piece (*PP*) of the spermatozoon tail; notice the Jensen's ring (*JR*) prevents the mitochondria from migrating down the principal piece (×30,000). Plasmalemma (*P*); nucleus (*N*)

with its various structural components tailored to specific aspects of function. At first glance, as in many other mammal species, the boar ejaculated spermatozoon can be divided into two major parts: (1) the head containing the cell DNA (haploid nucleus) and the mechanisms for sperm-oocyte recognition and subsequent fusion (acrosome) and (2) the tail concerned with sperm motility being the site of energy production (it contains mitochondria that generate the energy necessary for movement) and the propulsive apparatus for the initiation and maintenance of cell motility (axoneme); both regions can be further subdivided into a number of cellular components, each with its own functional correlate (Figs. 1.3 and 1.4). This compartmentalization is a critically important feature of the sperm structure enabling this cell to perform the variety of tasks it must undertake. The structural and ultrastructural characteristics of the different organelles and cytoskeletal elements of the boar ejaculated spermatozoon will be described in the following sections.

The mature boar spermatozoon is an elongated cell of about 43–45 μm in length (Briz 1994; Holt et al. 2010) with two major distinguishable regions, the head and the tail, separated by a short linking segment called the connecting piece (or neck). The head is bilaterally flattened and oval shaped, with the following dimensions: 7 μm in length, 3.7 μm at its widest point and 0.4 μm in thickness. The two surfaces of the head are not exactly the same; while one is almost completely flat, the other has a half moon-shaped apical protuberance (or apical ridge), 0.4 μm in width and extending 1.2 μm along the edges of the head. The tail has a filamentous and cylindrical shape and can be subdivided into three major regions: the midpiece (or mitochondrial region), the principal piece and the terminal piece. The midpiece is 9 μm in length and 0.7 μm. in diameter; the principal piece is 26.2 μm in length and 0.4 μm in diameter; finally, the terminal piece is 2.2 μm in length and 0.2 μm in diameter. The connecting piece is 0.7 μm in length per 0.5 μm in thickness and has a trapezoidal shape with the wider base (1.3 μm) in contact with the head and the narrower base (0.6 μm) toward the midpiece; a small ring-shaped protuberance (or postcephalic ring) can be observed in the zone closer

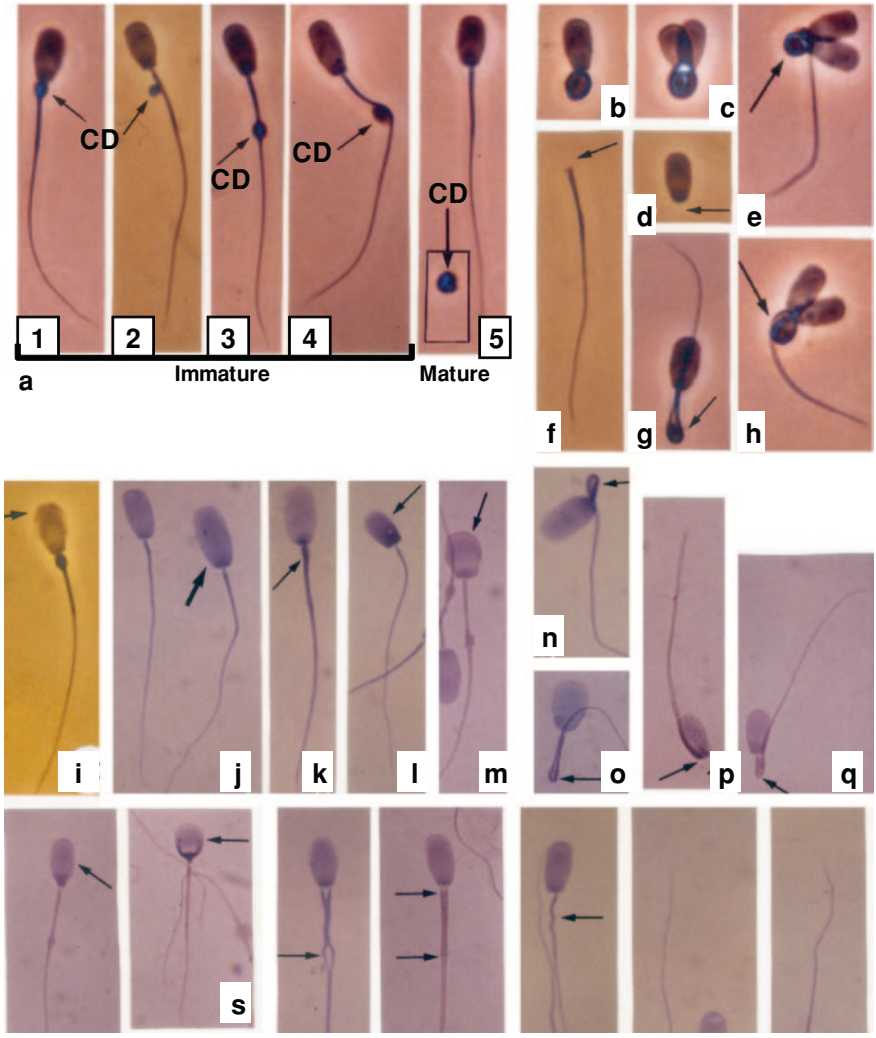

to the head (Fig. 1.6a) (Briz 1994; Bonet et al. 2000). Each of these regions and pieces has a distinct anatomy directly related to its function (Figs. 1.3 and 1.4).

1.2.2 Ultrastructure

The ultrastructural study is helpful because the electron microscope can actually display the structural elements of small cells like spermatozoon that light microscopy cannot reveal, i.e., there are a large number of ultrastructural abnormalities of boar ejaculates that can only be seen directly with electron microscopy. The two

◀ **Fig. 1.7** Positive phase-contrast (**a–i**) and bright-field (**j–z**) light micrographs showing immature, mature, and aberrant boar spermatozoa. **a** Migration and release of the residual cytoplasmic droplet (*CD*) during the process of epididymal sperm maturation: (*1*) immature spermatozoon with proximal CD; (*2*) immature spermatozoon with intermediate CD; (*3*) immature spermatozoon with distal CD; (*4*) immature spermatozoon with distal CD bending the tail before shedding the droplet; (*5*) mature spermatozoon just after having shed the CD. **b** Spermatozoon with intensely coiled tail. **c** Bicephalic spermatozoon with intensely coiled tail. **d** Tailless spermatozoon. **e** Bicephalic spermatozoon with tail coiled at the midpiece displaying a moderate intensity coiling (→). **f** Acephalic spermatozoon. **g** Immature spermatozoon with distal cytoplasmic droplet and tail folded at the Jensen's ring level (→). **h** Bicephalic spermatozoon with tail coiled displaying high intensity coiling (→). **i** Immature spermatozoon with damaged acrosome (→). **j** Mature spermatozoon and macrocephalic spermatozoon (→). **k** (→). Macrocephalic spermatozoon with thickened tail (→). **l** Microcephalic spermatozoon (→) with slightly shortened tail. **m** Immature spermatozoon with distal cytoplasmic droplet and round head (→). **n** Macrocephalic spermatozoon with tail folded at the midpiece level (→). **o** Macrocephalic spermatozoon with roundish head and tail folded at the Jensen's ring level (→). **p** Spermatozoon with tail folded at the connecting piece level (→). **q** Spermatozoon with tail folded at the midpiece level (→). **r** Immature spermatozoon with distal cytoplasmic droplet and a slightly thin head (→). **s** Spermatozoon with small and round head (→). **t** Spermatozoa displaying different intensities of tail coiling. **u** Spermatozoon with two fused tails (→). **v** Spermatozoon with two completely fused tails; notice the limits of the midpiece (→). **x** Spermatozoon with corkscrew defect affecting the midpiece (→). **y** Spermatozoon with tail folded at the midpiece (→). **z** Immature spermatozoon with proximal droplet and tail folded at the connecting piece level (→). (Magnification = ×1,400)

major regions of the boar mature spermatozoon, the head and the tail, as well as the connecting piece in between, will be considered in turn.

1.2.2.1 Head

The small and compact boar sperm head contains a very limited number of components; the only other major organelle in the head region, apart from the cell nucleus, is the acrosome. Neighboring structures are the postacrosomal dense lamina, the subacrosomal space, and the perinuclear fibrous material (Figs. 1.2a–c; 1.4a.1, a.2, b.1, b.2 and 1.5).

The nuclear shape determined by the sperm genotype is highly species-specific and most species show a very high degree of uniformity (Curry and Watson 1995). This is the case with the flattened ovoid-shaped nucleus of the ejaculated boar spermatozoon whose dimensions are 6.6 μm in length and variable in thickness at the proximal and distal cephalic regions (Figs. 1.1d, e and 1.5a, b); in the proximal region, the nucleus is 220 nm in thickness and in the distal region it is approximately 320 nm (Fig. 1.5b.1–b.5). The nucleus constitutes the major part of the sperm head, and as in many other mammalian species, it consists of a very rigid structure attributable to its extremely condensed and electrodense chromatin fibers.

Accompanying the nucleus is the sac-like acrosome, a membrane-bound vesicle that forms a cap over the anterior part of the nucleus covering approximately 80 % of its length (Fig. 1.5b). Two broadly parallel acrosomal membranes are considered in

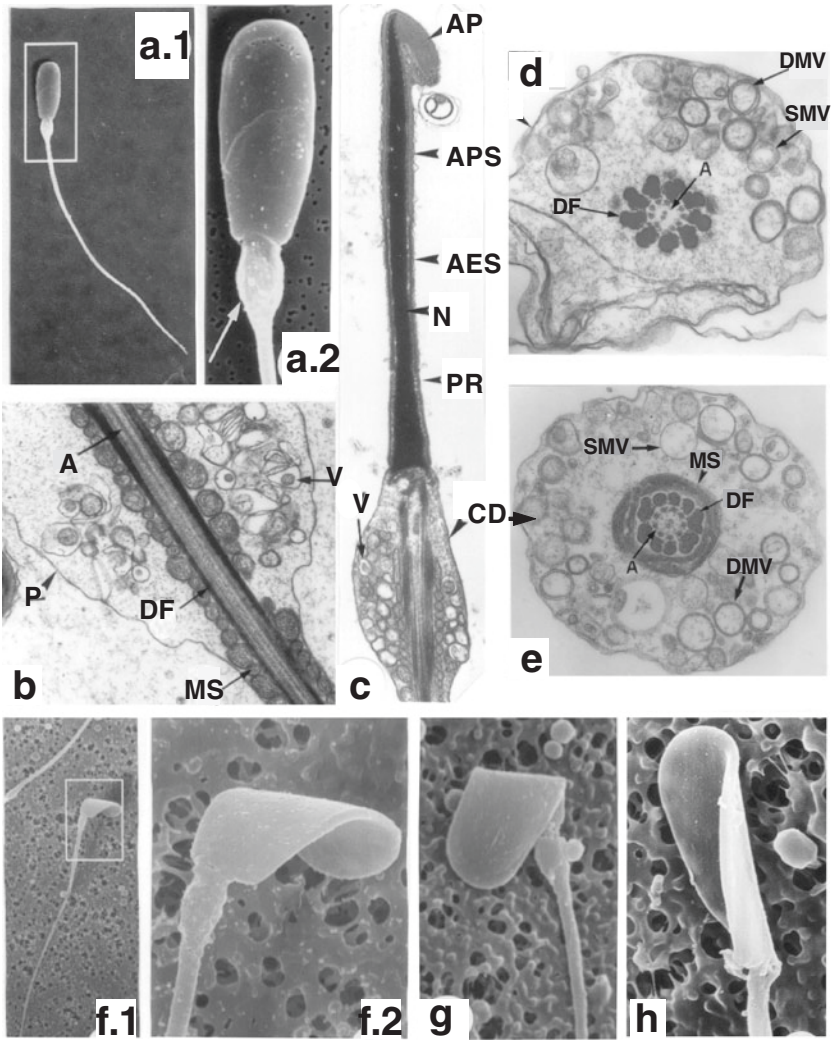

Fig. 1.8 Scanning (**a**, **f–h**) and transmission (**b–e**) electron micrographs showing the ultrastructure of the immature boar spermatozoa. **a.1** General view of an immature spermatozoon with proximal cytoplasmic droplet; the framed area is enlarged in figure **a.2** (×1,100). **a.2** Head and cytoplasmic droplet detail (→) (×4,400). **b** Longitudinal section through the cytoplasmic droplet; notice the abundant vesicles (*V*) (×24,000). **c** Longitudinal section of the head and the connecting piece; note the proximal cytoplasmic droplet (*CD*) (×13,000). **d** Cross section through the connecting piece showing double membrane vesicles (*DMV*) and simple membrane vesicles (*SMV*) inside the cytoplasmic droplet (×53,000). **e** Cross section through the cytoplasmic droplet; notice the midpiece occupies the droplet geometrical center (×60,000). Axoneme (*A*); acrosome equatorial segment (*AES*); acrosome principal segment (*APS*); acrosomal protuberance (*AP*); dense fibers (*DF*); mitochondrial sheath (*MS*); nucleus (*N*); plasmalemma (*P*); postacrosomal cephalic region (*PR*). **f.1** General view of an immature spermatozoon with proximal cytoplasmic droplet; the framed area is enlarged in figure **f.2** (×1,500). **f.2** Head transversely bent along its complete extension (×7,500). **g** Immature spermatozoon with proximal cytoplasmic droplet and the head transversely folded at the limit between the acrosomal and postacrosomal cephalic regions (×5,400). **h** Spermatozoon head rolled from its base (×6,500)

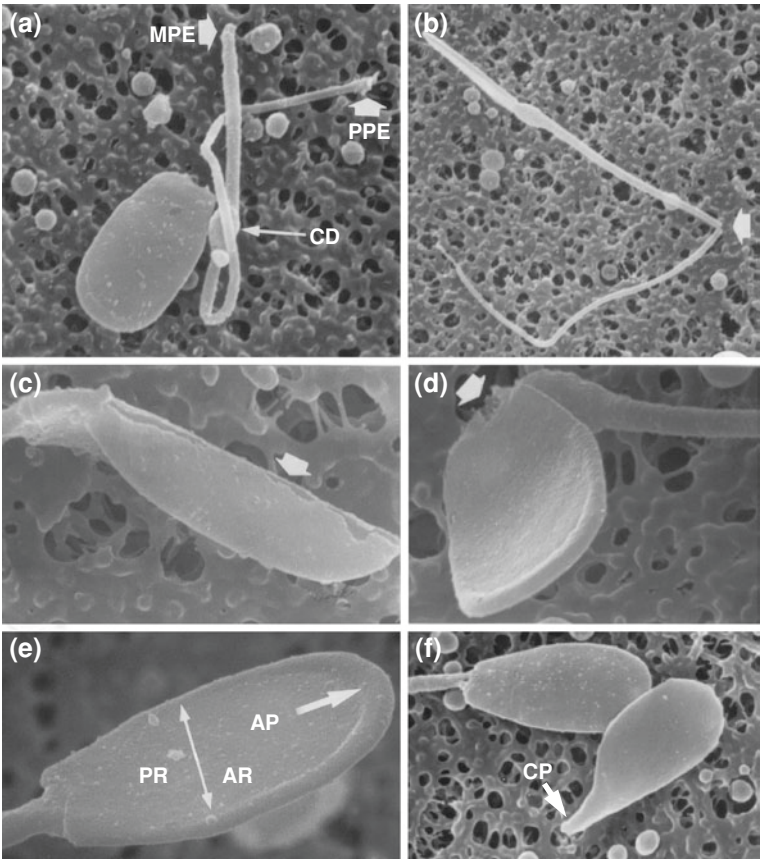

Fig. 1.9 Scanning electron micrographs showing characteristic malformations of the immature boar spermatozoa. **a** Separated head and tail of an immature spermatozoon with distal cytoplasmic droplet (*CD*); the tail's principal piece has been broken and has lost the terminal piece. midpiece proximal end (*MPE*); principal piece distal end (*PPE*) (×5,400). **b** Immature spermatozoon with proximal cytoplasmic droplet and tail broken at the point of the principal piece (→) (×3,600). **c** Immature spermatozoon with distal cytoplasmic droplet and head broken lengthwise (→) (×9,000). **d** Immature spermatozoon with proximal cytoplasmic droplet and head transversely broken (→) at its boundary with the cytoplasmic droplet (×9,000). **e** Detail of the head of an immature spermatozoon with distal cytoplasmic droplet; note the great development of the acrosomal protuberance (*AP*) which extends down to the boundary of the acrosomal region (→) (×9,500). Acrosomal region (*AR*); postacrosomal region (*PR*). **f** Spermatozoon with the tail broken at the beginning of the midpiece; note the severely pyriform head presents an intact connecting piece (*CP*) (×6,300)

this sac-like vesicle. An inner membrane overlays the nuclear envelope, which continues at the posterior margins of the acrosome forming an outer membrane lying directly beneath the plasmalemma. Enclosed inside these two acrosomal membranes is a narrow space, the acrosomal matrix, filled with amorphous material distributed

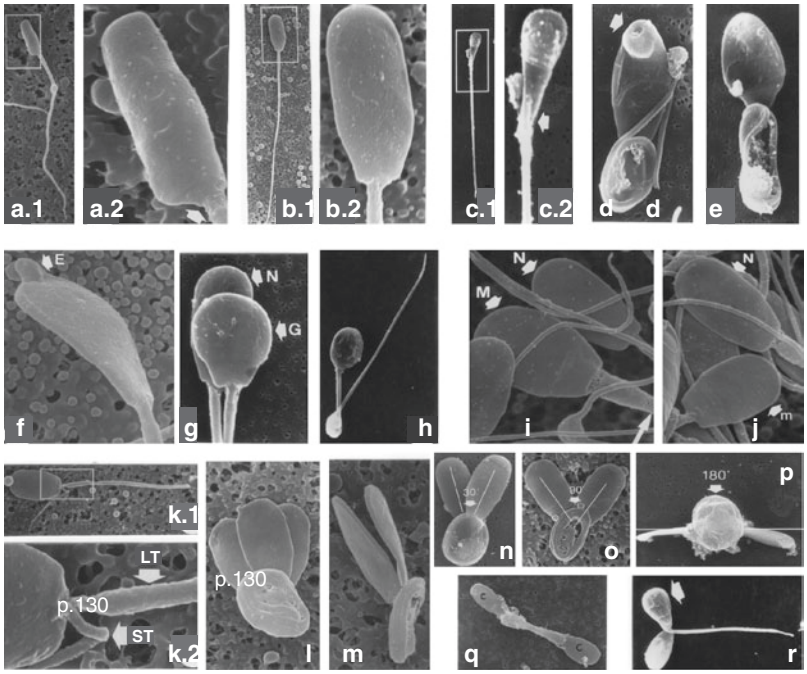

Fig. 1.10 Scanning electron micrographs showing different boar sperm malformations affecting the cephalic and the tail shape, size, and number. **a.1** General view of an immature spermatozoon with distal cytoplasmic droplet and abnormal head; the framed area is enlarged in figure **a.2** (×2,000). **a.2** Detail of the cylindrical or bacillary head displaying an abaxial tail attachment (→). (×8,000). **b.1** General view of a mature spermatozoon; the framed area is enlarged in figure **b.2** (×1,500). **b.2** Detail of the narrower and longer profile of the head (×6,000). **c.1** General view of a microcephalic mature spermatozoon; the framed area is enlarged in Figure. **c.2** (×1,500). **c.2** Detail of the elongated pear-shaped head; the *arrow* points to the head–tail junction (×6,000). **d** Coiled tail spermatozoon with a long flame-shaped head showing the craterlike appearance of the apical acrosomal protuberance (→) (×5,000). **e** Coiled tail spermatozoon with a short flame-shaped head (×5,400). **f** Spermatozoon with an apical acrosomal protuberance characterized by a well-developed knob (*E*) (knobbed acrosome defect) (×10,000). **g** Normal-headed spermatozoon (*N*) and spermatozoon with a globular head (*G*) (×5,000). **h** Folded tail spermatozoon with entirely roundish head (×2,600). **i** Macrocephalic spermatozoon (*M*) with two fused tails (→); note the normal spermatozoa (*N*) for size comparison (x5,400). **j** Microcephalic spermatozoon or with undersize head (**m**); note the normal-sized head (*N*) for comparison (×7,100). **k.1** General view of a macrocephalic spermatozoon with two unfused tails of different length and thickness; the framed area is enlarged in figure **k.2** (×1,500). **k.2** Detail of the cephalic region showing the attachment of the two tails, one of them short and thin (*ST*) and the other long and thick (*LT*) (×6,000). **l** Tricephalic spermatozoon with completely coiled tail (×4,400). **m** Side view of a bicephalic spermatozoon with a completely coiled tail; notice the two heads are overlapped on parallel planes (×5,600). **n** Spermatozoon with two heads on the same plane giving rise to about a 30º angle between them (×5,000). **o** Spermatozoon with two heads located on the same plane giving rise to about a 90º angle between them (×5,400). Notice in micrographs *n* and *o* that the completely coiled tail gives rise to a flattened structure which is on the same plane as the heads. **p** Spermatozoon with two heads on the same plane, but located in opposite directions giving rise to a 180º angle between them; note the coiled tail appears as a globular mass placed between the two heads (×3,000). **q** Spermatozoa with two uncoiled and antiparallel midpieces, and the principal and terminal pieces coiled over the midpieces; notice that one of the two heads is more voluminous than the other one (C, bigger head; c, smaller head) (×3,200). **r** Bicephalic spermatozoon with two uncoiled and fused tails; note the short tail and the pyriform shape of one of the two heads (→) (×2,500)

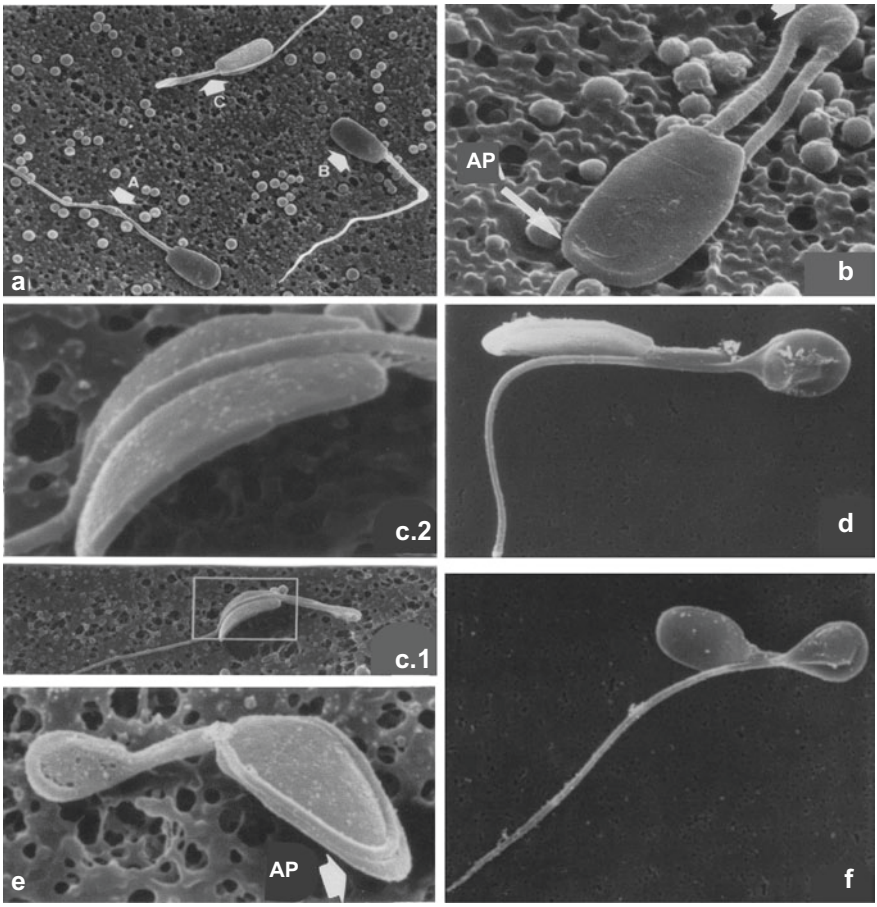

Fig. 1.11 Scanning electron micrographs showing different boar sperm malformations affecting the tail trajectory (*tail folding*). **a** Principal stages of tail folding at the location of Jensen's ring. *A*, immature spermatozoon with distal cytoplasmic droplet; *B*, immature spermatozoon with distal cytoplasmic droplet and its tail folded at Jensen's ring, displaying a 90º angle between the midpiece and the principal piece; *C*, immature spermatozoon with distal cytoplasmic droplet and a completely folded tail (×3,000). **b** Immature spermatozoon with distal cytoplasmic droplet (→); notice the 0º angle formed between the midpiece and the principal piece of the tail; in this phase of tail folding, these two pieces are not fused and the tail overruns the flat face of the head, leaving the cephalic face presenting the acrosomal protuberance (*AP*) uncovered (×5,000). **c.1** General view of a spermatozoon with its tail folded at Jensen's ring; the framed area is enlarged in figure **c.2** (×2,000). **c.2** Detail of the fusion of the principal piece along the midsagittal axis of the head; note the cephalic bending imprinted by the head and tail fusion (×8,000). **d** Spermatozoon with its tail folded at Jensen's ring; notice the cytoplasmic droplet consolidating the tail folding at Jensen's ring (×3,500). **e** Immature spermatozoon with a distal cytoplasmic droplet, a triangular-shaped head, its tail folded at the posterior third of the midpiece and coiled around the head, just below the acrosomal protuberance (*AP*) (×4,500). **f** Spermatozoon with its tail folded at the midpiece; notice that the tail is folded at the midpiece location because the zone affected by the bending shows a greater development than the kind which characterizes tail folding at Jensen's ring (×3,000)

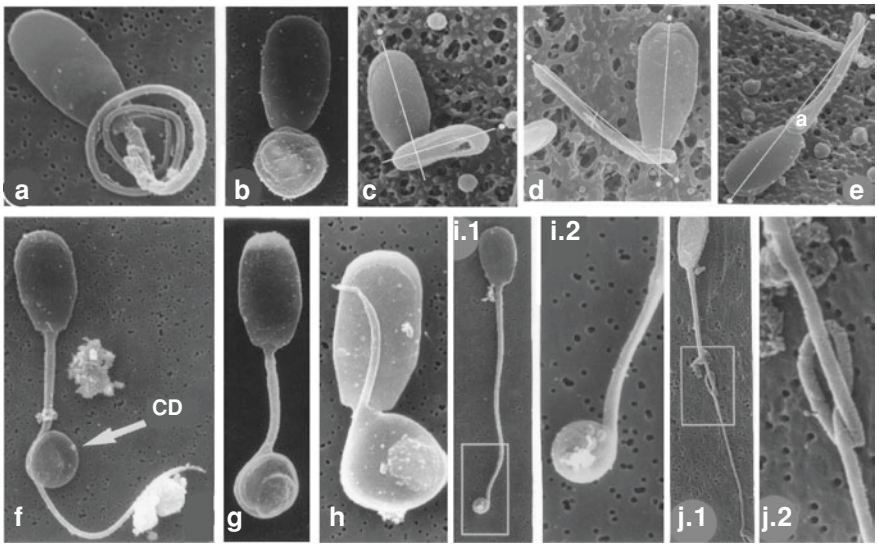

Fig. 1.12 Scanning electron micrographs showing different boar sperm malformations affecting the tail trajectory (*tail coiling*). **a** Spermatozoon with a coiled tail, but not fused; notice the tail turns in circles concentrically around itself (×6,800). **b** Spermatozoon with a coiled and fused tail (the plasmalemma covers the internal coiling of the tail); note the coiling displays a circular shape (×5,000). **c** Spermatozoon with a small elliptical head, along with an intensely coiled and fused tail; note the coiling displays an elliptical shape and is at 90º in regard to the midsagittal axis of the head (×5,200). **d** Spermatozoon with a coiled tail, giving rise to 45º angle in regard to the midsagittal axis of the head (×6,300). **e** Spermatozoon with its tail coiled along the entire midpiece; note the coiling begins by the tail folding at the Jensen's ring (×3,500). **f** Immature spermatozoon with its cytoplasmic droplet placed on the first segment of the principal piece; note that the principal piece displays a complete loop around the cytoplasmic droplet (*CD*) (×2,800). **g** Immature spermatozoon with its cytoplasmic droplet placed on the first segment of the principal piece; notice that the principal and terminal pieces turn completely around the cytoplasmic droplet (×3,000). **h** Spermatozoon with partially coiled tail; note the great development of tail coiling (×4,700). **i.1** Mature spermatozoon with its tail coiled at the distal end; the framed area is enlarged in figure **i.2** (×1,800). **i.2** Detail of the tail coiling which only affects the terminal piece and the distal segment of the principal piece (× 7,200). **j.1** General view of a spermatozoon with a false knot in the principal piece; the framed area is enlarged in figure **j.2** (×1,800). **j.2** Detail of the false knot of the principal piece (×7,200)

homogeneously and mostly corresponding to densely packed hydrolytic enzymes. The part of the head containing the acrosome is called the acrosomal region. Three acrosomal segments are clearly distinguishable: the apical segment, the principal segment and the equatorial segment; in this latter segment, the electrodensity of the acrosomal matrix is slightly higher than that of the first two segments. The acrosome apical segment is the most expanded zone of the vesicle, and this vesicular expansion does not have the same development in the two faces of the head; while in the non-flattened face of the head the apical segment stretches down to 0.72 μm in length per 270 nm at its widest point (Fig. 1.5b.1), in the flat face the apical segment reaches 0.50 μm in length per 100 nm at its widest point. The principal segment is 2.5 μm in

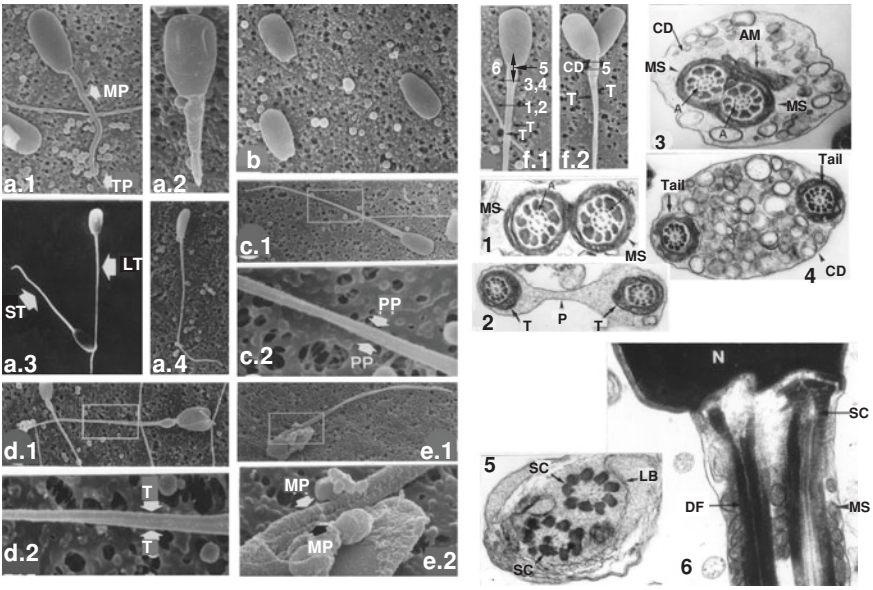

Fig. 1.13 Scanning and transmission electron micrographs showing different typologies of boar sperm malformations affecting the tail size and number. **a.1** Spermatozoon with short tail (14 m); note the tail presents the midpiece (*MP*)—that is longer than normal—and the terminal piece (*TP*), but not the principal piece (×3,600). **a.2** Spermatozoon with very short tail (7 m); notice the tail is thicker than normal and appears to be only formed by a short and thick midpiece (×4,500). **a.3** Spermatozoon with long tail (42 m) (*LT*) and spermatozoon with short tail (30 m) (*ST*) (×1,300). **a.4** Spermatozoon with long tail (43 m) (×1,400). **b** Tailless spermatozoa; note the tail breaking came about the base of the head (×2,700). **c.1** General view of an immature spermatozoon with proximal cytoplasmic droplet and two fused tails; the framed area is enlarged in figure **c.2** (×1,500). **c.2** Detail of the helix path of the two principal pieces (*PP*) (×6,100). **d.1** General view of an immature spermatozoon with proximal cytoplasmic droplet, with two heads and two fused tails; the framed area is enlarged in figure **d.2** (×1,500). **d.2** Detail of the principal piece region; note the two fused tails (*T*) (×6,000). **e.1** General view of a microcephalic spermatozoon with two fused tails; the framed area is enlarged in figure **e.2** (×1,500). **e.2** Detail of the initial region of the tail midpiece; notice the presence of two midpieces (*MP*) (×6,100). **f.1** General view of a spermatozoon with one head and two fused tails (*T*); the numbered arrows indicate the direction and the level of the sections depicted in Figs. 1.1–1.6 (×5,200). **f.2** General view of a spermatozoon with two heads and two fused tails (*T*); notice the residual cytoplasmic droplet (*CD*) (×5,200. (*1*) Cross section through the anterior region of the midpiece of a spermatozoon with two tails; note the mitochondrial sheaths (*MS*) coming in contact (×45,000). (*2*) Cross section through the mid-anterior region of the midpiece of a spermatozoon with two tails (*T*) (×36,000). (*3*) Cross section through the anterior region of the midpiece of a spermatozoon with two tails (*T*); notice the fused mitochondrial sheaths (*MS*) and the additional mitochondria (*AM*) (×42,000). (*4*) Cross section through the mid-anterior region of the midpiece of a spermatozoon with two tails (×36,000). (*5*) Cross section through the anterior part of the connecting piece of a spermatozoon with two tails (×45,000). (*6*) Frontal longitudinal section of a spermatozoon with one head and two fused tails (×33.000). Axoneme (*A*); cytoplasmic droplet (*CD*); nucleus (*N*); dense fibers (*DF*); laminar bodies (*LB*); mitochondrial sheath (*MS*); plasmalemma (*P*); segmented columns (*SC*)

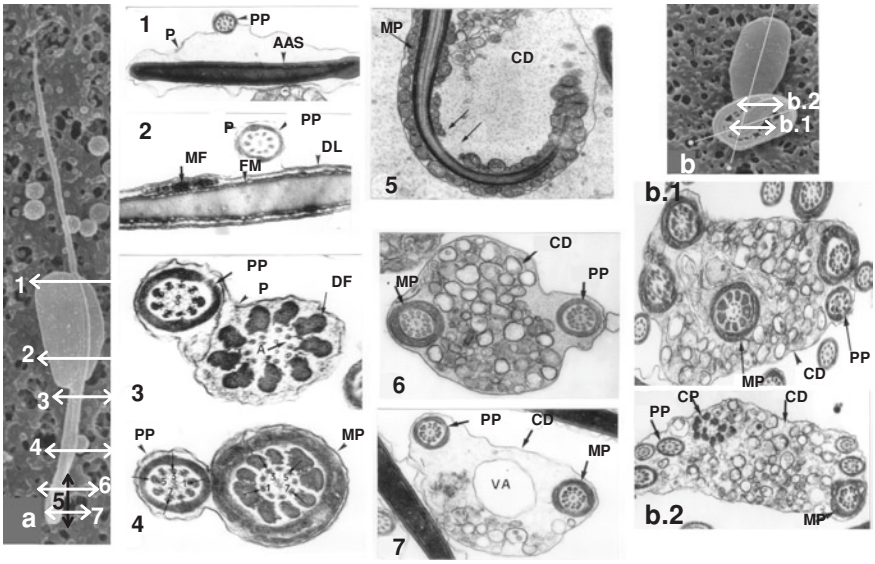

Fig. 1.14 Scanning and transmission electron micrographs showing different typologies of boar sperm malformations affecting the tail trajectory (*folded and coiled tails*). **a** General view of a spermatozoon with tail folded at the Jensen's ring; the *numbered arrows* indicate the direction and the level of the sections depicted in Figs. 1.1–1.7 (×6,400). (*1*) Cross section through the acrosome apical segment (*AAS*); note the plasmalemma (*P*) surrounds the acrosomal cephalic region and the tail principal piece (*PP*) (×25,000). (*2*) Cross section through the postacrosomal cephalic region; notice the myelin figures (*MF*) arranged between the postacrosomal dense lamina (*DL*) and the perinuclear fibrous material (*FM*) (×45,000). (*3*) Cross section through the posterior part of the connecting piece; note the proper organization of dense fibers (*DF*) and axoneme (*A*) (×85,000). (*4*) Cross section through the mid-anterior part of the midpiece (*MP*); notice the antiparallel disposition of the principal piece (*PP*) from the numbering of the axoneme microtubule doublets (×75,000). (*5*) Longitudinal section through the midpiece region (*MP*) where the tail folding occurs; note the disorganization of the mitochondrial sheath in this region (×30,000). (*6*) Cross section through the distal cytoplasmic droplet (*CD*) which consolidates tail folding (×30,000). (*7*) Cross section through the distal cytoplasmic droplet; notice the high vacuolation (*VA*) of the cytoplasmic droplet (×25,000). **b** General view of a spermatozoon with completely coiled tail; the *numbered arrows* indicate the direction and the level of the sections depicted in figures **b.1** and **b.2** (×8,100). **b.1** Section of a spermatozoon coiled tail; the midpiece (*MP*) appears in four sections and the principal piece (*PP*) in a single section (×25,000). **b.2** Section of a spermatozoon coiled tail at the connecting piece (*CP*) level (×22,000)

length in the flat face of the head and 2.8 μm in the other face; the thickness of this segment is about 80 nm. The equatorial segment is 2.3 μm in length, 40 nm in thickness in the two head faces, and 80 nm in thickness in the edges of the head.

The postacrosomal dense lamina consists of a homogeneous layer of fibrous and electrodense material, 1.4 μm in length and 25 nm in thickness, that lies parallel beneath the plasmalemma and takes up 20 % of the nuclear length, coinciding with the region of the nucleus not covered by the acrosomal vesicle (Figs. 1.4b.1, b.2 and 1.5b.4, b.5). The region of the head containing the postacrosomal dense

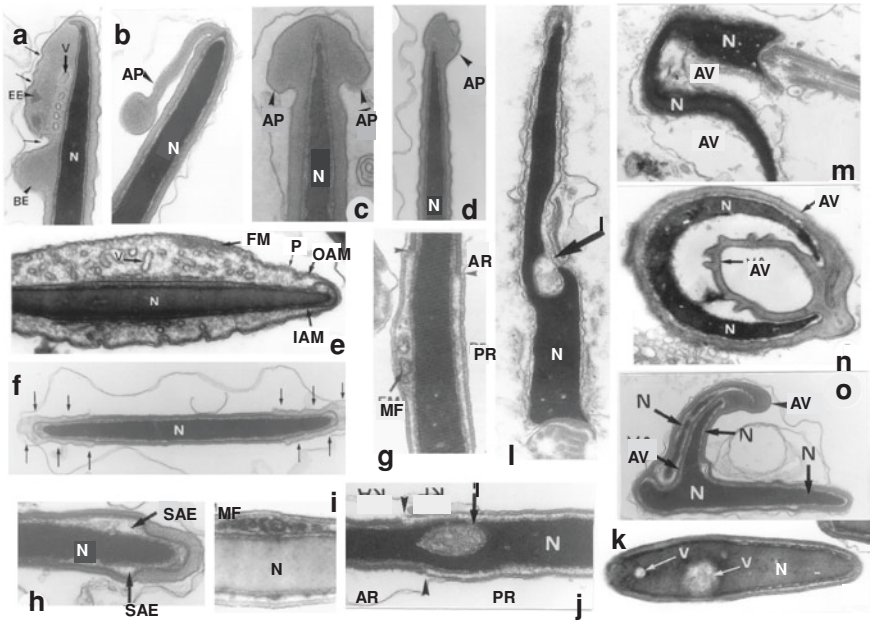

Fig. 1.15 Transmission electron micrographs showing different typologies of boar sperm cephalic malformations. **a** Longitudinal section of the acrosome apical segment; note the festooned perimeter of the acrosomal protuberance (→), the high inner vesiculation (*V*) and the matrix heterogeneity with highly electron dense zones (*EE*) and low electron dense zones (*BE*) (×50,000). **b** Longitudinal section of the acrosome apical segment; notice the drumstick-shape of the acrosomal protuberance (*AP*) (×40,000). **c** Longitudinal section of the acrosome apical segment; notice the symmetrical distribution of the acrosomal protuberance (*AP*) at both sides of the head (×63,000). **d** Longitudinal section of the acrosome apical segment; notice the scarce development of the drop-shaped acrosomal protuberance (*AP*) which is found in the cephalic apex (×25,000). **e** Cross section of the acrosome principal segment; notice the highly expanded acrosomal vesicle with a low matrix electron density and containing abundant vesicles (*V*) and electron dense fibrous material structures (*FM*). Inner acrosomal membrane (*IAM*); outer acrosomal membrane (*OAM*); plasmalemma (*P*) (× 45000). **f** Cross section of the acrosome equatorial segment; notice the festooned surface of the acrosomal vesicle at the end sides of the head (→) (×25,000). **g** Longitudinal section through the anterior postacrosomal region (*PR*) where myelin figures (*MF*) can be seen arranged only in the zone of the postacrosomal region closer to the acrosomal region (*AR*) (×46,000). **h** Cross section of the acrosome equatorial segment; note the high development of the subacrosomal space (*SAE*) (×30,000). **i** Cross section through the postacrosomal region where the myelin figures (*MF*) shows a linear arrangement which provokes a slightly protruding contour of the cephalic region (×80,000). **j** Longitudinal section through a spermatozoon head showing a false nuclear vacuole due to the refolding of the nuclear envelope within the invagination (*I*); note that this invagination is found in the anterior portion of the postacrosomal region (*PR*) closer to the acrosomal region (*AR*) (×37,000). **k** Cross section of the basal postacrosomal region; note the appearance of real non-membrane-bound nuclear vacuoles (*V*), thus being nuclear zones with low electron density due to the loosely compacted chromatin (×45,000). **l** Longitudinal section through a spermatozoon head showing a membrane-bound nuclear invagination giving rise to a false nuclear vacuole (*I*) (or nuclear pouche) (×32,000). **m** Longitudinal section of a spermatozoon with folded nucleus (*N*); notice the impaired appearance of the acrosomal vesicle (*AV*) (×24,000). **n** Cross section of a spermatozoon rolled head showing the curvature of the nucleus (*N*) and the appearance and placement of the acrosomal vesicle (*AV*) (×45,000). **o** Cross section of a spermatozoon with V-shaped nucleus (*N*) (or crested nucleus); note the appearance and placement of the acrosomal vesicle (*AV*) (×20,000)

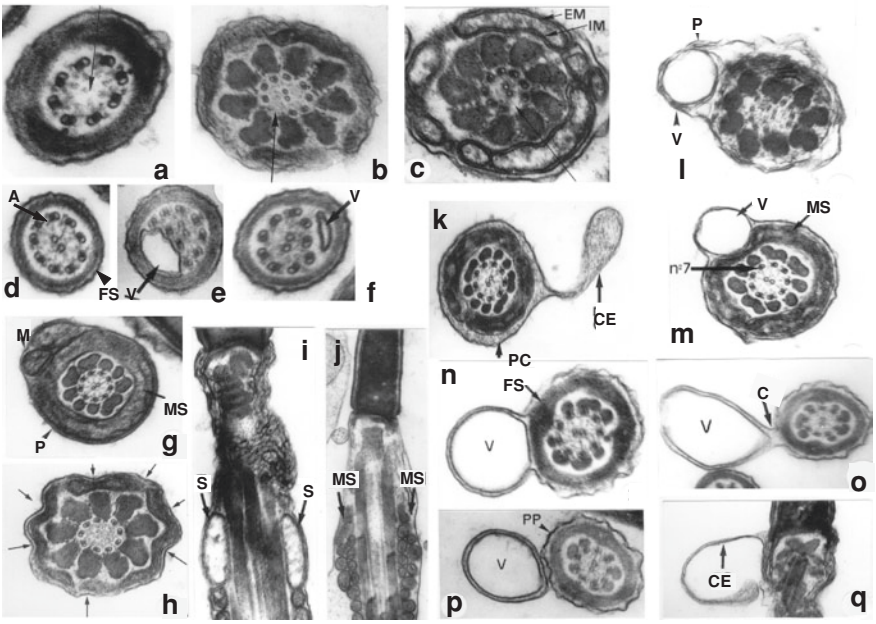

lamina is called the postacrosomal region. The plasmalemma enclosing the sperm head region overlays is firmly adhered to the postacrosomal dense lamina, but detaches very easily from the outer acrosomal membrane (Fig. 1.5b).

The subacrosomal (or perinuclear) space is the limit separating the nucleus from the inner acrosomal membrane or the innermost face of the postacrosomal dense lamina (Figs. 1.4a.1 and 1.5b.3–b.5). This space consists of a scarce electrodense matrix and a perinuclear fibrous material of greater electrodensity. The subacrosomal space is especially developed in the region beneath the acrosome apical segment; in this supranuclear region this space has a conical shape, with a base of 80 nm in diameter and 120 nm in length (Figs. 1.2a and 1.5b, b.1). The subacrosomal space is reduced to 25 nm in thickness along the acrosome principal segment, and in the two faces of the head; in contrast, it increases up to 40 nm in thickness along the acrosome equatorial segment and also in the two faces of the head, and comes to its maximum development in the postacrosomal region (70 nm) (Fig. 1.2b). The subacrosomal space increases considerably in the borders of the head (70 nm) corresponding to the acrosome principal and equatorial segments (Fig. 1.5b, b.2, b.3); in contrast, in the margins of the head corresponding to the postacrosomal region it is practically non-existent and the perinuclear fibrous material becomes connected with the postacrosomal dense lamina (Fig. 1.5b, b.4, b.5).

Finally, the perinuclear fibrous material (or subacrosomal fibrous material) consists of an electrodense layer coating the nucleus with a separation of 15 nm between them. The maximum development of this layer is found in the postacrosomal region, reaching about 15 nm in thickness, whereas in the acrosomal region

◀ **Fig. 1.16** Transmission electron micrographs showing different typologies of boar sperm tail malformations. **a** Cross section through the mid-posterior region of the principal piece showing the absence of the central microtubule pair (→) of the axoneme (×140,000). **b** Cross section through the anterior region of the midpiece showing the absence of the peripheral microtubule doublet number 9 (→) (×100,000). **c** Cross section through the anterior region of the midpiece showing the absence of the peripheral microtubule doublet number 8 (→); note the extreme swelling of the mitochondrial sheath, and that the inner mitochondrial membrane (*IM*) has no type of folding, and is parallel to the outer mitochondrial membrane (*EM*) (×80,000). **d** Cross section through the mid-posterior region of a normal principal piece where a complete axoneme (*A*) can be observed inside the fibrous sheath (*FS*) (×140,000). **e** and **f** Cross sections through the mid-posterior part of the principal piece; note the presence of cytoplasmic vacuoles (*V*) which provoke an axonemal deformation affecting the peripheral microtubule doublets 4, 5 or 6 (figure **e**, ×61,000; figure f, ×70,000). **g** Cross section through the mid-region of the midpiece; note the presence of some additional mitochondria (*M*) located between the plasmalemma (*P*) and the mitochondrial sheath (*MS*) (×60,000). **h** Cross section through the anterior region of the midpiece; notice the festooned contour (→) attributable to the lesser thickness and greater fragility of the mitochondria which form the mitochondrial sheath (×70,000). **i** Longitudinal section of the connecting piece and the anterior region of the midpiece; note the great swelling (*S*) of the first mitochondria of the mitochondrial sheath (×45,000). **j** Longitudinal section of the connecting piece and the anterior region of the midpiece; note the arrangement of the double layer of mitochondria forming the mitochondrial sheath (*MS*) (×40,000). **k** Cross section through the posterior region of the midpiece; notice the highly developed peripheral cytoplasm (*PC*) and the formation of a great digitiform cytoplasmic evagination (*CE*) (×45,000). **l** Cross section of the connecting piece showing the presence of a voluminous vacuole (*V*) located below the plasmalemma (*P*) (×60,000). **m** Cross section through the mid-region of the midpiece; note the presence of a voluminous vacuole (*V*) located in front of the peripheral microtubule doublet number 7, which provokes a noticeable deformation on the mitochondrial sheath (*MS*) (×75,000). **n** Cross section through the anterior region of the principal piece; note the presence of a voluminous vacuole (*V*) and that the fibrous sheath (*FS*) provokes a slight deformation of the circular perimeter of the vacuole (×90,000). **o** Cross section through the anterior region of the principal piece; note the process of the shedding of the vacuole (*V*), which only maintains contact with the principal piece by a slender thread of cytoplasm (*C*) (×47,000). **p** Cross section through the anterior region of the principal piece showing the loss of contact between the vacuole (*V*) and the principal piece (*PP*) (×75,000). **q** Longitudinal section of the connecting piece; note the formation of a vacuole caused by the folding of a digitiform cytoplasmic evagination over itself (*CE*); this cytoplasmic evagination is found in the region of the boundary between the head and the connecting piece (×45,000)

this layer is thinner and poorly condensed showing less electrodensity (Figs. 1.2a–c; 1.4b.1, c and 1.5b, b.4, b.5).

1.2.2.2 Connecting Piece

The connecting piece (or neck) of the boar spermatozoon is a short linking segment between the base of the nucleus and the first mitochondrion of the tail midpiece (Figs. 1.3, 1.4c, 1.6a–e). It firmly attaches itself to the distal end of the head, being trapezoid in shape (Figs. 1.4c and 1.6a). The outline of the plasmalemma along the connecting piece and the postacrosomal cephalic region shows a slight circular neckline (or postcephalic ring) just in the head–tail junction (Figs. 1.2d

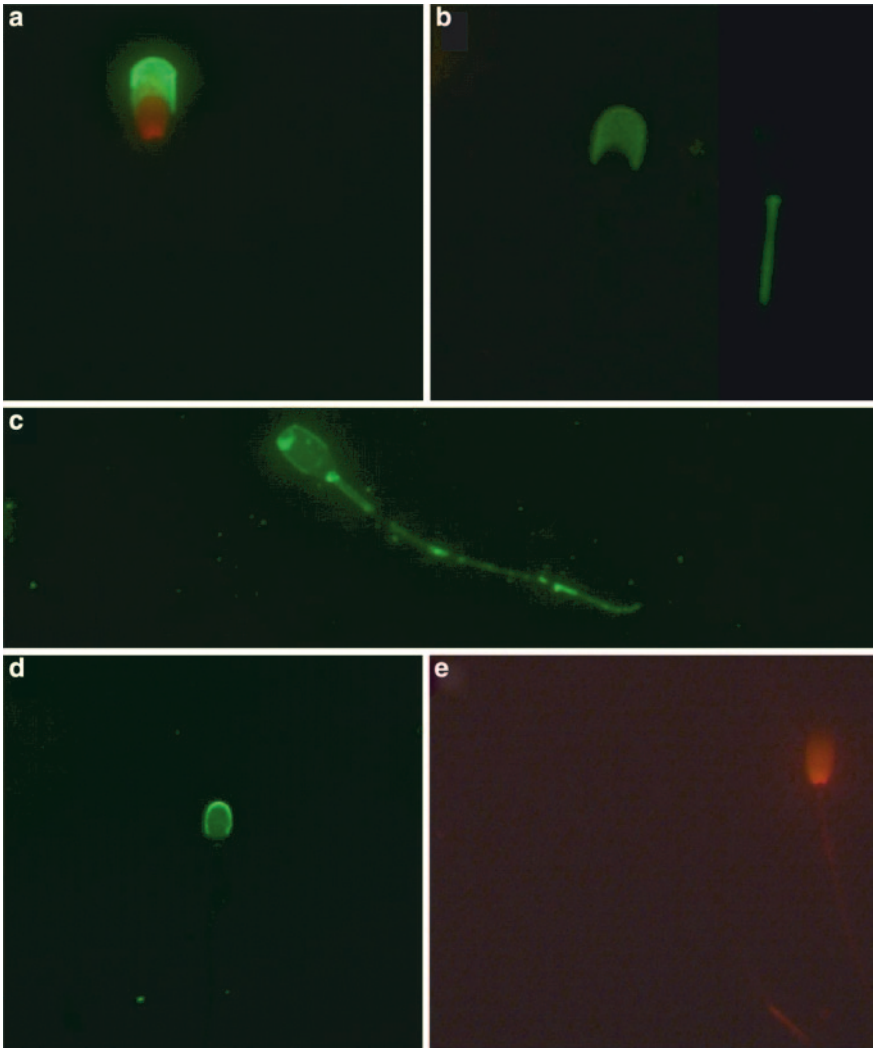

Fig. 1.17 Fluorescence micrographs of boar spermatozoa from epididymal cauda for galactose (**a**), glucose/mannose (**b**), N-acetyl-D-glucosamine (**c**), N-acetyl-D-galactosamine (**d**) and fucose moieties (**e**). **a** Galactose residues (FICT-PNA lectin) expressed over a membrane-damaged spermatozoa (PI labeled) with reacted acrosome (×600). **b** Glucose/mannose residues (FICT-PSA lectin) expressed over the acrosome and mitochondrial sheath (×600). **c** N-acetyl-D-glucosamine residues (FICT-WGA) expressed over the whole sperm surface (×600). **d** N-acetyl-D-galactosamine residues (FICT-SBA) expressed over the apical ridge (×400). **e** Fucose residues (TRITC-UEA-I) expressed over the acrosome and mitochondrial sheath (×400)

and 1.6a, b). Its major components are: the basal plate, the laminar bodies, the capitulum, the segmented columns, the basal body, and the axoneme (Fig. 1.4c).

The basal plate consists of an electrodense material very similar to that of the postacrosomal dense lamina lying at the caudal surface of the nucleus, and which

extends along about 0.6 μm (30 nm thick), adhered to the outer membrane of the nuclear envelope (Figs. 1.2d and 1.6d).

The laminar bodies come from pronounced folds of redundant nuclear envelope and enclose chromatin-free nuclear space. These folds have cylindrical disposition with walls of 150 nm in thickness, arise from the perimeter of the nuclear base and extend along 1.2 μm, terminating at the first mitochondrion of the tail midpiece (Figs. 1.2d, e, 1.6b, d).

The capitulum is a dome-shaped structure lying beneath the basal plate and separated from it by approximately 40 nm. The segmented columns arise from the capitulum ends and go down to the tail midpiece. The capitulum and also the segmented columns are electrodense structures of about 130 nm in thickness. While the laminar bodies are attached to the mitochondrial sheath of the tail midpiece, the segmented columns are attached to the outer dense fibers of the tail midpiece (Fig. 1.2d).

The nine segmented columns are individualized at the more distal end of the capitulum (0.3 μm of distance from it) (Fig. 1.6d and e). Along the first 0.3 μm of distance, the segmented columns fuse between them, and therefore, it is more proper to refer to them as capitulum extensions than as columns. The individualized segmented columns are cylinder-shaped and stretch along 0.8 μm down to the midpiece, enclosing the axoneme in a cylindrical space of 220 nm in diameter (Figs. 1.2e and 1.6e). These columns present two types of cross-striations with alternate periodicity; one type eminent and the other type less well defined. The distance between two consecutive eminent striations is 80 nm, and between an eminent striation and the consecutive less well defined striation, 40 nm (Fig. 1.6c).

The basal body is located at the feet of the convexity defined by the capitulum and the segmented columns, i.e., a space of 220 nm in diameter and 260 nm in height. It is positioned at an angle of 45º with respect to the longitudinal axis of the spermatozoon (Fig. 1.6d). The microtubular triplets of the basal body are arranged in small depressions of the capitulum which indicate the limits of the segmented columns drafts. This basal body marks the origin of the axoneme, which stretches progressively throughout the full length of the spermatozoon tail. The respective nine evenly spaced peripheral microtubule doublets of the axoneme are surrounded by the nine segmented columns, which in turn are surrounded by the laminar bodies (Fig. 1.2e).

1.2.2.3 Tail

Higher vertebrates have a noteworthy complexity in sperm tail organization showing the presence of a significant number of additional structures to the axoneme as compared to the invertebrate species (Curry and Watson 1995). Three regions are clearly distinguishable in the boar spermatozoon tail: the midpiece (or mitochondrial region), the principal piece and the terminal piece (Figs. 1.3, 1.4 and 1.6f–h).

The midpiece of the spermatozoon tail stretches from the distal end of the connecting piece to the annulus or Jensen's ring, an electrodense band marking the junction of the midpiece and the principal piece (Fig. 1.6b, g, i). The major structures of the midpiece are: the axoneme, the mitochondrial sheath, the outer dense fibers (or coarse fibers) and the peripheral granules (Figs. 1.2d, f and 1.4d.1, d.2). The axoneme occupies the central axis of the midpiece and has the classic 9 + 2 microtubular pattern, with the characteristic axoneme elements (dynein arms, nexin links, radial spokes, connecting bridge, and central sheath) (Figs. 1.2f and 1.4d.2). The nine peripheral microtubule doublets are numbered 1–9 in a clockwise direction, with number 1 being the only doublet situated on a plane perpendicular to that of the two central microtubules. As mentioned above, the axoneme stretches along the full length of the three pieces of the spermatozoon tail (midpiece, principal, and terminal pieces) (Figs. 1.2d–i and 1.4d–h). The mitochondrial sheath lies directly beneath the plasmalemma and consists of several elongated mitochondria (150 nm in diameter) lying end to end in a helical arrangement around the underlying axoneme. This sheath is approximately 80 nm thick. The mitochondrial matrix consists of very electrodense material and the crests lie parallel to the double mitochondrial membrane (Figs. 1.2f and 1.4d.1, d.2). The outer dense fibers (or coarse fibers) are filamentous cytoskeletal structures consisting of electrodense material lying between the mitochondrial sheath and each of the peripheral microtubule doublets of the axoneme. The dense fibers extend along the whole midpiece and the first third of the principal piece. Maximum thickness and diameter of the dense fibers are found in the distal end of the connecting piece and they decrease progressively along the two following pieces. Individual dense fibers, numbered by their association with the microtubular doublets of the axoneme, have a characteristic shape in cross section, all of them acquiring a truncated pyramid-like form with the narrower base toward the microtubular doublets and the wider base, round-edged, toward the mitochondrial sheath (Figs. 1.2f and 1.4d.2, e). The dense fibers are not all of equal thickness and diameter. In the proximal region of the midpiece, fibers number 1, 5, and 6 average 110 nm in thickness and 150 nm in diameter, and fibers number 2, 3, 4, 7, 8 and 9 average 80 nm in thickness and 110 nm in diameter. In the distal region of the midpiece, fibers number 1, 5 and 6 average 160 nm in thickness and 40 nm in diameter, and the remaining fibers average 70 nm in thickness and 60 nm in diameter. The peripheral granules distributed in the interstices between the outer dense fibers are only found in the proximal region of the midpiece. They consist of electrodense granules, of 15 nm maximum diameter, which disappear progressively as the dense fibers reach the distal region of the midpiece (Fig. 1.2f).

The principal piece is the longest segment of the spermatozoon tail, extending from the annulus or Jensen's ring to the proximal end of the terminal piece (Fig. 1.4e, f, g.1, g.2). The principal piece is characterized by the presence of: the fibrous sheath, the outer dense fibers, the axoneme, and the Jensen's ring. The fibrous sheath of the principal piece has a very high electrodensity, and replaces the mitochondrial sheath of the midpiece. It consists of two continuous longitudinal axes or columns (dorsal and ventral) coplanar with the central

microtubule pair; these two columns are joined by a series of circumferential ribs regularly distributed around the principal piece (Fig. 1.4e). The fibrous axes lie between the plasmalemma and the dense fibers 3 and 8 (Fig. 1.4f). The axes reach their maximum thickness (110 nm) at the first third of the principal piece and they decrease progressively along the following two thirds until being equal to the ribs' thickness (75 nm). Along the first third of the principal piece the great development of the axes determines their overlying and fusion with the dense fibers 3 and 8 beyond the termination of these fibers; thus, the axes continue attached to their underlying microtubule doublets (Fig. 1.4f). The remaining dense fibers, which stretch only along the first third of the principal piece, decrease progressively in thickness until they disappear. The two posterior thirds of the principal piece differ from the first third by their lack of dense fibers and because the thickness of the fibrous axes equals that of the fibrous ribs (75 nm) (Fig. 1.4g.1, g.2). The fibrous ribs are approximately 15 nm apart and about 40 nm in diameter along the whole principal piece. The thickness of the ribs, together with that of the axes, decreases progressively as the fibrous sheath draws nearer the terminal piece. The annulus or Jensen's ring consists of an electrodense ring-shaped structure underlying the plasmalemma, marking the junction of the midpiece and the principal piece. The plasmalemma is firmly attached to the Jensen's ring and this separates the mitochondrial sheath from the fibrous sheath. The Jensen's ring links up with the last mitochondrion of the mitochondrial sheath and is detached from the first ribs of the fibrous sheath by approximately 15 nm. This structure is about 130 nm thick and 160 nm in diameter (Fig. 1.6g, i).

The terminal piece is the last and shorter segment of the spermatozoon tail and has no accessory cytoskeletal structures, consisting only of the axoneme enclosed by the plasmalemma (Figs. 1.3, 1.4 and 1.6f, h). Whereas in other tail pieces the plasmalemma has a more or less smooth circular outline, in this last piece it adopts a festooned appearance. The axoneme becomes progressively disorganized as it stretches down the principal piece, with the B microtubule being the first element to disappear; finally, the microtubular disorganization makes it impossible to distinguish the typical axonemal 9 + 2 pattern (Fig. 1.4h).

1.3 Sperm Malformations

The careful study of structural and ultrastructural details in boar ejaculated spermatozoa has greatly assisted the development of an improved systematic classification for sperm malformations. Thus, an electron microscopic examination of sperm can be diagnostically helpful in case the source of a fertility alteration cannot be identified by means of other analyses.

Boar sperm malformations, understood as the whole range of immature and aberrant gamete forms, can have their origin in the testis (primary malformations) or in the epididymis (secondary malformations) (Bonet et al. 1992; Briz 1994; Briz et al. 1995, 1996).

1.3.1 Classification

The percentage of mature spermatozoa in a normal boar ejaculate is between 80 and 95 %; the percentage of immature spermatozoa ranges from 5 to 15 %; and the percentage of sperm malformations or aberrant spermatozoa is between 1 and 5 % (Martin 1982; Briz 1994; Bonet et al. 2000).

Among other features (described below), the immature spermatozoon mainly differs from the mature spermatozoon by the presence of a residual cytoplasmic droplet. This droplet consists of the remains of residual cytoplasm made redundant toward the end of spermiogenesis (see Sect. 3.2.3). It can be found at the connecting piece level or at a variable level along the midpiece, because the droplet forms at the connecting piece and moves down the midpiece, being released just at the Jensen's ring level of the spermatozoon (Fig. 1.7a) during the process of epididymal sperm maturation (see Sect. 3.3.4). Hence, the cytoplasmic droplet has two end positions: the proximal position (when placed at the connecting piece) (Fig. 1.7a.1, i, z) and the distal position (when placed at the Jensen's ring) (Fig. 1.7a.4, m, r). In domestic species, if the droplet is normally shed, then its retention on sperm in the ejaculate may be associated with infertility, and there is considerable evidence that this is the case; most reports relate the retention of proximal droplets (at the connecting piece) to be indicative of a failure of normal epididymal maturation (Cooper and Yeung 2003; Cooper 2005). All boar ejaculates show spermatozoa with residual cytoplasmic droplets but not all must be a priori considered abnormal; a distinction must be drawn between proximal and distal cytoplasmic droplets. Only, the immature spermatozoa with proximal cytoplasmic droplet are classified as sperm malformations in boar ejaculates, since this is a clear sign of a default in maturation that may cause impairment of the sperm fertilizing capacity under natural conditions. It has been demonstrated that ejaculates with more than 5 % of proximal cytoplasmic droplets produce a decrease in fertility; in contrast, there is no direct correlation between the percentage of distal cytoplasmic droplets and fertility (Gonzalez-Urdiales et al. 2006). However, Waberski et al. (1994) reported that infertility characterized by reduced pregnancy rate and litter size was also associated with retention of the distal droplet (at the Jensen's ring) in boars, although proximal droplets were also retained in these males. Immature sperm with proximal cytoplasmic droplet originate in the testis and this droplet normally moves distally, during passage through the epididymis, until it reaches the Jensen's ring and, once these spermatozoa with distal cytoplasmic droplet reach the epididymal cauda, they shed the cytoplasmic droplet and take on the appearance of mature spermatozoon (Fig. 1.7a.1–a.5). Therefore, the greater or lesser incidence of immature spermatozoa with proximal cytoplasmic droplet in the boar ejaculate enables us to determine the degree of sperm epididymal maturation. Inadequate or poor sperm epididymal maturation correlates with the inability to fertilize the oocyte due to shortcomings in sperm motility and/or interaction and fusion processes between the spermatozoon and the oocyte. Moreover, the presence of retained cytoplasmic droplets in ejaculated

spermatozoa may also be considered as a primary failure originated in the testes involving a membrane defect, and makes it difficult later on for the cytoplasmic droplet to migrate from the connecting piece to the end of the midpiece during epididymal maturation (Cooper and Yeung 2003; Cooper 2005). In conclusion, in boars, as in other mammalian species, the presence of a high percentage of abnormal spermatozoa with cytoplasmic droplets in their ejaculates has been related to poor fertility (Waberski et al. 1994; Cooper 2005; Gonzalez-Urdiales et al. 2006), lower binding capacity to oviductal explants (Petrunkina et al. 2001), and chromatin instability (Ardón et al. 2008).

The classification of sperm malformations may be carried out taking into account the external or internal morphology of the ejaculated spermatozoon, as well as their site of origin (Briz 1994; Briz et al. 1995; Bonet et al. 2000). Even though spermatozoa malformations are classified with regard to one aberrant sperm structure, often several abnormal structures converge in the same spermatozoon. Macrocephaly or microcephaly, additional heads or tails, longer or shorter tails, different shape malformations of the head, folding or coiling of the tail, etc. can be malformations found in the same aberrant spermatozoon (Fig. 1.7). Theoretically, there can be as many typologies of aberrant spermatozoa as paired combinations of the several possible malformations. Therefore, it is common to observe aberrant spermatozoa that, besides the highlighted malformation, present a second abnormality (e.g. aberrant spermatozoa with two or three heads and coiled tail, with macrocephaly and folded tail or two tails, with a flame-shaped head and coiled tail, etc.) (Figs. 1.7c, e, h, n, o and 1.10d, e, k–q). In order to establish a methodology for the description of the different morphological incidences it is useful to establish a classification criterion of cephalic malformations (affecting shape, size and number) and tail malformations (affecting shape or trajectory, size, and number), which frequently appear simultaneously. Moreover, the different aberrations present in the ejaculate may also be classified, in accordance with their place of origin, as primary or secondary: (1) primary malformations are those developed in the testis during spermatogenesis or spermiogenesis, and (2) secondary malformations are those developed during the sperm maturation process along the epididymis. In general, cephalic and tail size and number malformations tend to be of primary origin, but those affecting the tail trajectory are usually of secondary origin. Other malformations can be observed as a result of processing ejaculates in the laboratory (see Sect. 4.4.4).

Therefore, and according to the external and internal morphology of spermatozoa the following types of sperm malformations can be observed more or less frequently in boar ejaculates: immature spermatozoa with proximal cytoplasmic droplet (Figs. 1.7, 1.8 and 1.9); sperm malformations affecting the cephalic shape, size, and number (Figs. 1.7 and 1.10); and, sperm malformations affecting the tail trajectory, size, and number (Figs. 1.7, 1.11, 1.12 and 1.13). They are described one by one in the next section, some of them accompanied by ultrastructural details as seen by transmission electron microscopy (spermatozoa with two fused tails, with tail folded at the Jensen's ring, with coiled tail and with cephalic and tail malformations) (Figs. 1.7, 1.13, 1.14, 1.15 and 1.16).

1.3.2 Structure and Ultrastructure

The immature boar spermatozoon presents three distinctive traits compared to the mature spermatozoon: presence of the residual cytoplasmic droplet, greater development of the acrosome apical protuberance (or apical ridge) and greater flexibility of the head (Figs. 1.7a.1, i; 1.8 and 1.9).

The residual cytoplasmic droplet is approximately 1.5 μm in diameter and habitually encloses a small segment of the midpiece and contains an electrolucent cytoplasm rich in vesicles (Fig. 1.8a–c). The midpiece can be located at the center of the droplet or much more displaced from the center. The number and development of the vesicles increase as the cytoplasmic droplet moves distally from the connecting piece and along the midpiece (Fig. 1.8c–e). Two types of vesicles can be observed: double membrane vesicles and simple membrane vesicles. Double membrane vesicles have a clear matrix and a constant diameter of approximately 0.2 μm; they come from the cisternae of the smooth endoplasmic reticulum which close up over themselves enclosing hyaloplasmic material. Simple membrane vesicles also have an electrolucent matrix and arise from expansions of the endoplasmic reticulum. These last vesicles fuse together giving rise to greater vesicles exhibiting a large variety of diameters ranging from 0.1 to 0.9 μm (Fig. 1.8d, e).

The acrosome apical protuberance (or apical ridge) shows more development in immature than in mature spermatozoa. Its external width and length in the mature spermatozoon are 400 nm and 1.2 μm, respectively (Fig. 1.5a); and they increase until 600 nm and 4.5 μm, respectively, in the immature spermatozoon (Fig. 1.9e).

The head of the immature spermatozoa has greater flexibility than on reaching maturity. Different types of folds and deformations are often observed in the head of the immature spermatozoa. The more or less intense cephalic folds occur frequently through a cross plane (Fig. 1.8f, g), and more rarely through a frontal longitudinal plane (Fig. 1.8h). The most common cephalic malformation is a slight lateral deviation of the acrosomal region of the head with regard to the longitudinal axis of the cell. The immature spermatozoon is fragile, so it is not rare to observe transverse or longitudinal broken heads and tail ruptures (Fig. 1.9a–f).

Spermatozoa with malformations affecting the cephalic shape, such as elongation and flame, oval and round shapes, can be observed through light microscopy (Fig. 1.7m, r, s, u). The higher resolution of the scanning electron microscope, as compared to conventional light microscopy, allows for a more accurate detection of such anomalies (Fig. 1.10).

Two main types of spermatozoa with elongated heads can be found: spermatozoa with cylindrical heads and spermatozoa with narrow heads. Spermatozoa with elongated and cylindrical heads, about 8 μm in length and 2.7 μm in diameter, are characterized by an abaxial tail attachment (Fig. 1.10a). Spermatozoa with elongated and narrow heads, about 9–10 μm in length and 3.5–4.1 μm in diameter, are characterized by a normal tail attachment (Fig. 1.10b). Likewise, one can distinguish spermatozoa with elongated pear-shaped heads, detectable by the scarce development of the acrosomal cephalic region and the narrower postacrosomal region (Fig. 1.10c).

Spermatozoa with flame-shaped heads can also be classified regarding two major typologies: short flame-shaped heads and long flame-shaped heads (Fig. 1.10d, e). In this last typology, the apical ridge acquires a crater-like appearance (Fig. 1.10d).

Spermatozoa with oval heads usually present an apical acrosomal knob of variable development (Fig. 1.10f). Spermatozoa with round heads display many typologies ranging from globular to flat shapes and exhibiting different degrees of roundness (Fig. 1.10g, h).

With regard to the size of the head, two types of spermatozoa can be observed: macrocephalic and microcephalic spermatozoa (Figs. 1.7j–l, n, o, s and 1.10i, j). Within the macrocephalic or giant head spermatozoa, two typologies can be found: spermatozoa with normal head length (7 μm) and large width (4.7 μm), and spermatozoa with longer (7.7 μm) and wider (5.5 μm) heads. This last type of spermatozoa often has two tails (Fig. 1.10k). Within the microcephalic or small head spermatozoa, two typologies can also be noted: spermatozoa with normal head width and reduced length (5.2 μm), and spermatozoa with shorter (4.5 μm) and narrower (2.4 μm) heads.

Spermatozoa with more than one head frequently have as many fused tails as heads; these tails often exhibiting different degrees of coiling. Among spermatozoa with more than one head, those with three heads and those with two heads can be distinguished. Tricephalic spermatozoa tend to present completely coiled fused tails and three positioned coplanar heads giving rise to an angle not greater than 30º between them (Fig. 1.10l). Bicephalic spermatozoa tend to present completely or partially coiled fused tails and two heads arranged in coplanity in crossed planes (Figs. 1.7c, e, h and 1.10m, q). When the two heads are coplanar an angle ranging from 0º (overlapped heads) to 180º (opposite heads) can be formed between them (Fig. 1.10n–p). In this last case, heads are fused at their bases or they are separated by the tail coiling. When the two heads are positioned in crossed planes, these are orthogonal. In general, the two heads are often flat-shaped and attached to the connecting piece ending. However, a flat-shaped head and a globular or pyriform head can be found in some bicephalic spermatozoa (Fig. 1.10r). Head-to-head and tail-to-tail agglutinations are the possible origins of spermatozoa with more than one head.

Depending on the type of malformation affecting tail bending, one can distinguish two types of spermatozoa: spermatozoa with folded tails and spermatozoa with coiled tails.

Folding of tails can occur at the Jensen's ring level, at the midpiece level or at the connecting piece level. A tail folding is considered an anomaly when the tail bends completely in a way that the two parts of the folded tail run antiparallel (Figs. 1.11 and 1.14a). The most habitual folding occurs in immature spermatozoa with distal cytoplasmic droplet at the Jensen's ring level (Figs. 1.7g, o, 1.10h and 1.11a–d). The tail bends in the form that the principal piece contacts and fuses with the midpiece initially and with the flat face of the head later; finally, the tail can coil and fuse progressively over the flat face of the head (Figs. 1.11c–e and 1.14a). A more uncommon folding can also be observed; it concerns spermatozoa

whose tails bend at the midpiece level (Figs. 1.7n, q, y). This folding tends to be very apparent because of the midpiece thickness and the cytoplasmic droplet diameter and, in some cases, could be confused with a spermatozoon head under light or scanning electron microscopy due to its size and shape (Fig. 1.11d–f). The last category of spermatozoa with tail folded at the connecting piece level is even rarer and is scarcely found in boar ejaculates (Fig. 1.7p, z).

Spermatozoa with coiled tail exhibit complete or partial coiling (Fig. 1.7b, c, e, h, t). The most typical form is that of spermatozoa whose tails wrap around the first half of the midpiece (Fig. 1.12a). Within this modality, several typologies can be identified in regard to the placement of the coiling with respect to the head, and to the size and shape of this coiling. The coiling size may vary from approximately one half of the head size (Fig. 1.12b) to that of a normal-sized head (Fig. 1.12c, d). This variability relies on the degree of coiling and on the length of the coiled tail (depending on whether any tail piece is missing or is shorter). Moreover, the major axes of tail coiling and those of the head may be arranged in such a way as to give rise to angles of 180º, 90º, 45º or 30º (Fig. 1.10n–q). Tail coiling may adopt circular, spherical, oval or elliptical shapes. A second type of tail coiling is that of spermatozoa whose tails twist around the whole midpiece. In this case, the tail coiling adopts a very clear elliptical shape. The major axis of the coiling and the major axis of the head may be arranged so as to give rise to angles of 180º, 90º or 45º. Finally, more unusual tail coiling forms can be observed, for instance: coiling affecting solely the principal piece (Fig. 1.12f), coiling involving the principal and terminal pieces (Fig. 1.12g), coiling impacting the midpiece and partially the principal piece (Fig. 1.12h), coiling affecting solely the terminal piece or also partially the principal piece (Fig. 1.12i), false coiling (Fig. 1.12j), etc.

There are two modalities of sperm malformations affecting tail size: spermatozoa with short tails and spermatozoa with long tails (Fig. 1.13a). When the spermatozoon tail is shorter than normal it is generally due to the absence of some piece or to the lesser development of one of them; the affected piece is often the principal one (Fig. 1.13a.1, a.2). When the spermatozoon tail is longer than normal it is habitually due to a longer principal piece (Fig. 1.13a.3, a.4).

Two types of malformations affecting the tail number can be distinguished: tailless spermatozoa (Figs. 1.7d, 1.9f and 1.13b) and spermatozoa with two tails (Figs. 1.7u, v, 1.10k and 1.13c–e). The first typology is characterized by the presence of detached heads in the ejaculate; the majority of these forms correspond to artifactual breaking of heads and tails during handling that are often concentrated at the edges of the semen smears. Therefore, this malformation is really determined by the count of detached heads minus the number of detached tails. Spermatozoa with two tails may be classified according to whether the two tails have the same length or not, and whether they are fused or not (Figs. 1.10k and 1.13c–e). Moreover, it is also possible to find spermatozoa with two heads and with two completely fused tails (Fig. 1.13d).

Regarding the type of ultrastructural malformation, as observed on transmission electron micrographs, aberrant boar spermatozoa can also be classified into: (1) spermatozoa with two fused tails, (2) spermatozoa with tail folded at the

Jensen's ring, (3) spermatozoa with coiled tail, (4) spermatozoa with cephalic malformations, and (5) spermatozoa with tail malformations.

Spermatozoa with two fused tails have two complete axonemal axes (Figs. 1.7v and 1.13f). The two axonemal axes run parallel along their full path (Fig. 1.13f.5, f.6). Depending on the region examined one can find: (a) the two axonemal axes separated by a highly developed cytoplasmic mass (Fig. 1.13f.2, f.4), or (b) the two axonemal axes in contact with their respective mitochondrial and fibrous sheaths (Fig. 1.13f.1, f.3). Residual cytoplasm, actually abundant from the connecting piece to the intermediate region of the midpiece, declines considerably as it reaches the distal end of the midpiece.

Spermatozoa with tail folded at the Jensen's ring consolidate the folding by means of the distal cytoplasmic droplet (Figs. 1.7g, 1.10a–c and 1.14a.5–a.7). Beyond the distal cytoplasmic droplet domain, the principal piece and the midpiece overrun antiparallel (Fig. 1.14a). The fibrous and mitochondrial sheaths of both pieces come into contact, and the fibrous sheath provokes a slight deformation on the mitochondrial sheath in the proximal end of the midpiece. The principal piece overruns the midpiece following a helix path which becomes apparent by the evolution of the series of doublets faced between the midpiece and the principal piece (Fig. 1.14a.4). Along the postacrosomal cephalic region, the principal piece lies between the plasmalemma and the postacrosomal dense lamina (Fig. 1.14a.2). Along the acrosomal cephalic region, the principal piece is located between the plasmalemma and the acrosomal vesicle (Fig. 1.14a.1).

Spermatozoa with coiled tail have an axonemal axis that traces several loops inside a cytoplasmic mass rich in double membrane vesicular elements and the remainder of smooth endoplasmic reticulum (Fig. 1.14b). Such cytoplasm morphology is very similar to that of the cytoplasmic droplet of an immature spermatozoon. The axonemal axis is positioned at the periphery of the cytoplasmic mass (Fig. 1.14b.1). Degenerated cell figures can also be observed and characterized by their cytoplasmic plasmolysis and by the absence of some microtubular structures of the axonemal axes (Fig. 1.14b.1, b.2).

Spermatozoa with ultrastructural cephalic malformations consist of abnormalities affecting the different acrosomal segments, the postacrosomal cephalic region and the nucleus.

The acrosome apical segment may display several malformations: high or low development, anomalous shapes and distributions, internal vesicalization and heterogeneous acrosomal matrix (Fig. 1.15a–d). The acrosome principal segment can exhibit the following aberrations: acrosomal vesicle expansion, scarce matrix electrodensity, and vesicalization (Fig. 1.15e). The acrosome equatorial segment can also present different malformations: high development of the subacrosomal space, and expanded and festooned edges of the acrosomal vesicle (Fig. 1.15f, h).

In the postacrosomal region, a greater or lesser development of myelin fibers between the postacrosomal dense lamina and the perinuclear fibrous material can be found (Fig. 1.15g, i).

Finally, the most typical ultrastructural nuclear anomalies are membrane-bound nuclear invaginations and nuclear vacuoles (Fig. 1.15l, j, k). Moreover, other

nuclear malformations can also be observed (e.g. nucleus folded by a longitudinal or by a transverse axis) accompanied by acrosomal anomalies (generally, vesicalization or plasmolysis) (Fig. 1.15m–o).

Spermatozoa with ultrastructural tail malformations affect the axoneme, the mitochondrial sheath and the perimitochondrial cytoplasm (Fig. 1.16).

Several modalities of axonemal anomalies consisting of the absence of microtubular elements can be detected: deficiency of the peripheral microtubule doublets (6, 8, 9 and, 5, and 6) and absence of the central microtubule pair (Fig. 1.16a–c). Furthermore, we can also observe a general disorganization and deformation of the axonemal structure by the presence of more or less developed vesicles lying between the fibrous sheath and the axoneme (Fig. 1.16d–f).

The two main ultrastructural abnormalities affecting the mitochondrial sheath are mitochondrial swelling (Fig. 1.16c) and the irregular arrangement of the mitochondria in the sheath (Fig. 1.16g). Mitochondrial swelling affects generally the first mitochondria of the mitochondrial sheath (Fig. 1.16i). These mitochondria can be five times greater in diameter compared to the others in the sheath and be characterized by a very clear matrix and by the absence of mitochondrial cristae. The inner mitochondrial membrane does not form cristae and runs parallel to the outer membrane (Fig. 1.16c). The other alteration of the mitochondrial sheath consists of an anomalous distribution of mitochondria. In this case, there are additional mitochondria regularly distributed in a helix path external to the sheath which determine a slight deformation of the circular perimeter of the midpiece (Fig. 1.16g, j). Moreover, the mitochondrial sheath sometimes exhibits reduced thickness and a festooned contour (Fig. 1.16h).

Concerning the perimitochondrial cytoplasm, several ultrastructural malformations may be highlighted. Peripheral vesicalization can be found at any level of the first three tail pieces of the spermatozoon disturbing the circular perimeter of the tail, the development of the vesicles being greater from the connecting piece to the principal piece. At the connecting piece level, peripheral vesicles (about 0.30 μm in diameter) lie between the laminar bodies and the plasmalemma (Fig. 1.16l). At the midpiece level, vesicles (about 0.35 μm in diameter) lie between the mitochondrial sheath and the plasmalemma, provoking a noticeable deformation on some mitochondria (Fig. 1.16m). At the principal piece level, vesicles (about 0.40 μm in diameter) lie between the fibrous sheath and the plasmalemma and do not provoke noteworthy deformations on the fibrous sheath ribs (Fig. 1.16n). These vesicles are released along the proximal region of the principal piece by narrowing at their base and the posterior fusion of the plasmalemma (Fig. 1.16o, p). These vesicles may come from large vesicles within the cytoplasmic droplet of immature spermatozoa or from cytoplasmic expansions present in the connecting piece or midpiece of some spermatozoa. The residual cytoplasm appears under two forms at the connecting piece and midpiece level: (a) in the form of cytoplasmic expansions and (b) in the form of perimitochondrial cytoplasmic films. The cytoplasmic expansions lie at the base of the head, just in the junction of the connecting piece and the postacrosomal cephalic region (Fig. 1.16q). They are digitiform cytoplasmic evaginations, 1 μm in length per

0.1 μm in diameter, filled with a homogeneous and slightly electrodense cytoplasm. These evaginations may bend until fusing at their free end with the plasmalemma enclosing the connecting piece, and remain attached or are occasionally released. Digitiform or fungiform cytoplasmic evaginations can also be found at the more distal region of the midpiece. In these cases, the cytoplasmic expansion arises from a highly developed perimitochondrial cytoplasmic film (Fig. 1.16k).

In any case, most of the defects described above prevent proper sperm function, either impairing motility (tail malformations) or causing weaknesses in sperm-oocyte interaction (cephalic malformations).

1.4 Sperm Cell Surface

The mature spermatozoon is a highly polarized cell with a minimal amount of cytosol and organelles, which has lost its potential for gene expression and, consequently, for protein synthesis (there are no ribosomes and chromatin is extremely condensed and tightly packed) (Boerke et al. 2007). This seems to make mammalian spermatozoa proteomically simpler than somatic cells. However, the spermatozoon has a highly complex degree of plasma membrane specialization and more membrane proteins than many other cell types. In addition, spermatozoa undergo significant post-testicular maturation in the epididymis and reorganization during capacitation in the female reproductive tract in order to acquire their complete functionality to fertilize the oocyte (Brewis and Gadella 2010). Epididymal maturation and fertilizing ability acquisition convert the sperm plasma membrane into a very dynamic structure, with polarized domains of intramembranous particles, subjected to several modifications by the releasing, the redistribution or the adsorption of proteins and lipids that change the lipid/protein ratio and composition (Flesch and Gadella 2000).

As a result of these cell surface modifications, occurring from spermatogenesis to fertilization, the mature spermatozoon emerges as a highly polarized and differentiated cell which shares some cell surface similarities with other highly differentiated cell types such as epithelia, photoreceptors, and neurons (Thaler and Cardullo 1995). Like many cells involved in recognition, binding and signaling events, the mammalian spermatozoon exhibits a high degree of molecular mosaicism on its surface, which applies not only to the membrane proteins but also to the lipid environment as well (for a detailed review see Jones et al. 2007, 2008). According to the pattern of the membrane, the sperm surface may be considered to have five major membrane domains, each closely associated with an underlying cell compartment or cytoskeletal element and involved in different aspects of cell function. The head has three major domains covering the acrosomal region in its three distinguishable segments (the apical ridge, and the principal and equatorial segments), and the tail has distinct domains over the midpiece and the principal piece (Figs. 1.4 and 1.5).

This regional membrane specialization allows the underlying cellular components to interact independently with their external environment, thereby enabling

efficient performance of the various tasks necessary for successful fertilization (i.e. recognition, binding and fusion with the oocyte) (Curry and Watson 1995). In particular, the acrosome apical region of the sperm head specifically recognizes and binds to the oocyte zona pellucida; the acrosome principal region is involved in the acrosome reaction required for zona penetration; and the acrosome equatorial region specifically recognizes and fuses with the oocyte plasma membrane. Despite the fact that the surface of the midpiece and principal piece of the sperm tail are also hetereogeneous, the function of these plasma membrane specializations is not yet understood but it is likely that these domains are involved in the organization of optimal sperm motility characteristics (Brewis and Gadella 2010).

1.4.1 The Glycocalyx

Mammalian spermatozoa are covered by a carbohydrate-rich dense coating zone. Several hundred different glycoproteins comprise the sperm glycocalyx forming a 20–60 nm thick coat essential for the acquisition of full sperm fertilizing ability. The mature glycocalyx becomes an immunoprotective barrier for the spermatozoa in the female tract, allows intercellular gamete communication and has an important role in the early interaction steps during sperm-oocyte recognition (Kirchhoff and Hale 1996; Schroter et al. 1999; Flesch and Gadella 2000; Diekman 2003). Some of these sugar residues are synthesized within the testis, while others are produced in the efferent ducts, by the epididymis epithelium or by the accessory glands, and incorporated during the spermatozoa post-testicular maturation.

The carbohydrate residues are linked to proteins and lipids of the sperm membrane. Sugar residues can be intercalated or anchored within the lipid bilayer, or superficially associated with the membrane via polar groups or through hydrophobic interactions. They can be either integrated within the sperm membrane or loosely associated with it (Schroter et al. 1999).

Lectins are, commonly, proteins of plant origin and are able to recognize specific oligosaccharide structures. The conjugation of lectins with fluorochromes or biotin systems permits cell-surface sugars and the changes that these sugars undergo during cell growth, differentiation or malignancy, to be investigated (Lis and Sharon 1998). This association is also useful for the structural characterization of the carbohydrate moieties of glycoproteins, as lectins can discriminate different glycoconjugates in the spermatozoon surface. Several studies have been performed with lectins to analyze the carbohydrate composition of sperm plasma membrane in species such as rodents (Brown et al. 1983; Liu et al. 1991; Tulsiani et al. 1993; Calvo et al. 1995); poultry (Pelaez and Long 2007), rabbits (Nicolson et al. 1977), marsupials (Cooper et al. 2001), monkeys (Navaneetham et al. 1996; Srivastav 2000), rams (Hammerstedt et al. 1982; Magargee et al. 1988), bovine livestock (Taitzoglou et al. 2007), stallions (Desantis et al. 2010), porcine livestock (Harayama et al. 1998; Jiménez et al. 2002, 2003) or humans (Kallajoki et al. 1985; Bains et al. 1992).

The glycocalyx carbohydrate composition of the sperm surface is strongly modified throughout the epididymis and the net negative surface charge increases (López et al. 1989). Most lectins intensely label almost every part of the sperm surface, illustrating the importance of the glycocalyx around the spermatozoon. The principal piece of the boar spermatozoon is only coated by N-acetyl-D-glucosamine and N-acetyl-galactosamine residues (Fàbrega et al. 2011a). The global galactose, glucose/mannose, and N-acetyl-D-glucosamine content increases significantly over the surface throughout the epididymal duct, whereas N-acetyl-D-galactosamine and fucose residues are maintained in spermatozoa coming from the proximal regions of the epididymis and slightly decrease in those from the epididymal cauda (Fàbrega et al. 2011a). These changes are probably mediated by the secretion of specific sialoproteins into the epididymal corpus lumen of boars (Harayama et al. 1999) and their arrangement over the sperm surface (Calvo et al. 2000), which can mask sperm surface carbohydrate residues during examinations.

The specific location of the different carbohydrate residues throughout the epididymis has been also studied. Galactose residues are practically absent over the intact acrosome surface and they are localized mostly over the outer acrosomal membrane (Fazeli et al. 1997) and over the cytoplasmic droplet and midpiece of immature boar spermatozoa from the epididymal caput (Fig. 1.17a) (Fàbrega et al. 2011a). Galactose residues are also found to be abundant over the cytoplasmic droplet of bull and ram epididymal spermatozoa (Arya and Vanha-Perttula 1985; Magargee et al. 1988) and they could probably be involved in cytoplasmic droplet migration along the spermatozoon tail midpiece during the process of epididymal sperm maturation (Fàbrega et al. 2011a) (see Sect. 3.3.4). Fucose residues are rarely detected on the epididymal boar sperm surface and they are only significantly observed on spermatozoa from the epididymal corpus (Fig. 1.17e). This exclusive distribution may respond to the secretion of specific sialoproteins into the epididymal lumen (Harayama et al. 1999). In contrast, N-acetyl-glucosamine residues are highly spread over the sperm surface (Fig. 1.17c), especially over the flagellum and over the apical ridge in boar spermatozoa coming from distal epididymal regions and ejaculates (Töpfer-Petersen et al. 2008; Fàbrega et al. 2011a). Glucose/mannose residues are principally located over the sperm acrosomal surface and over the sperm tail midpiece throughout the epididymis (Fig. 1.17b). The N-acetyl-galactosamine residues intensely coat the acrosomal apical ridge (Fig. 1.17d) and the cytoplasmic droplet surface of boar epididymal sperm (Wagner et al. 2002; Fàbrega et al. 2011a). As can also be observed for several sperm surface proteins (Phelps et al. 1990; Petruszak et al. 1991), the migration of these residues toward the sperm head during maturation (Wagner et al. 2002; Fàbrega et al.2011a) is consistent with their involvement in the capacitation process of ejaculated boar sperm (Jiménez et al. 2003), in sperm-oocyte interaction (Nimtz et al. 1999; Töpfer-Petersen 1999), and in the prevention of head-to-head sperm agglutination (Calvo et al. 2000). Furthermore, oligomannose or mannosyl residues are specifically known to have an important role in the creation of the sperm reservoir in pig oviducts (Wagner et al. 2002).

A study performed by our group with different lectins has demonstrated changes in the composition of the carbohydrate moieties that coat the sperm surface glycoproteins during the epididymal transit for sperm maturation. Among the most visible, a 112–102 kDa glycoprotein, which exhibits galactose, glucose/mannose, N-acetyl-glucosamine, N-acetyl-galactosamine and fucose moieties, is present throughout the entire epididymal transit; a 151 kDa glycoprotein containing glucose/mannose, N-acetyl-glucosamine, and fucose moieties has been identified only in spermatozoa from the proximal caput; a 133 kDa glycoprotein with fucose moieties is present from the distal caput to the cauda; multiple glycoproteins from 91 to 73 kDa with N-acetyl-glucosamine, N-acetyl-galactosamine, and fucose moieties are only present on proximal and distal caput epididymal spermatozoa; three glycoproteins of 16, 19 and 23 kDa with glucose/mannose moieties appear in succession along the epididymal regions and could represent transient forms of a same protein for which glycans are modified during the epididymal transit (Fàbrega et al. 2011a). These complex modifications on the sperm surface during maturation are the consequence of several interactions with the epididymal milieu, in particular with glycosidases, known to be present at elevated concentrations in this medium (Syntin et al. 1996).

During boar sperm capacitation and acrosome reaction the glycocalyx composition and distribution over the sperm surface is also hardly modified. The presence of N-acetyl-glucosamine residues over the sperm head and flagellum in epididymal spermatozoa decreases in the ejaculated spermatozoa after capacitation and even further after the acrosomal reaction. Glucose/mannose residues mainly increase over the acrosomal region in capacitated spermatozoa and are concentrated over the apical ridge in the acrosome-reacted sperm. Furthermore, fucose residues are scarcely present over ejaculated, capacitated, and acrosome-reacted spermatozoa as previously described for the epididymal spermatozoa (Jiménez et al. 2003).

1.4.2 Features of Boar Sperm Membrane Proteins and Lipids

It has been suggested that boar sperm protein and lipid composition are found in similar total amounts, the phospholipid/protein weight ratio of an isolated plasma membrane being approximately 0.68 (Nikolopoulou et al. 1985). However, spermatozoa epididymal transit and capacitation change both ratio and composition (Flesch and Gadella 2000).

Sperm plasma membrane proteins play a key role in sperm–oocyte interaction. Several changes in the protein composition of the sperm surface membrane occur during post-testicular differentiation, maturation of spermatozoa throughout the epididymal transit, storage in the epididymal cauda and in the female tract. Also, several seminal plasma proteins, such as sperm surface protein DQH and several seminal plasma spermadhesins such as porcine seminal plasma glycoprotein (PSPII), spermadhesins with N-terminal amino acid sequence Ala–Gln–Asn

(AQN-1 and AQN-3) and with N-terminal amino acid sequence Ala–Trp–Asn (AWN) and their respective glycoslyated isoforms (Sanz et al. 1991; Jonáková et al. 2000) are known to bind the sperm surface during maturation or to participate at ejaculation in the sperm reservoir in the porcine oviduct (Manásková et al. 2007), in sperm capacitation and to assist primary sperm interactions with the zona pellucida (Petrunkina et al. 2000). Boar spermadhesins are synthesized by the epididymis and the accessory glands of the male genital tract, and some of them, such as AWN, also in the Fallopian tube of the female genital tract (Ekhlasi-Hundrieser et al. 2002). Calcium-binding proteins (CBPs) are other boar seminal plasma proteins that bind specifically during epididymal transit onto the boar sperm plasma membrane that overlies the principal segment and which are known to be removed during capacitation (Peterson et al. 1989).

Epididymal maturation results in the progressive disappearance of most of the testicular compounds on the boar sperm surface membrane, which are either renewed or masked by new permanent or transient low molecular weight polypeptides (Dacheux et al. 1989) and processed according to their specific function: (1) proteins located to specific domains, such beta-fertilin (ADAM2) or PH-20 are processed and relocated (Primakoff et al. 1985; Overstreet et al. 1995; Blobel 2000) in order to participate in oocyte–sperm interaction and fecundation (Jury et al. 1997; McLaughlin et al. 1997; Waters and White 1997); (2) some proteins secreted by epithelial epididymal cells are apparently added to the sperm surface (Gupta 2005), such as MEPs or SMA-4 in mice, E-3 in rats, HEP64 or P26 h in other rodents, and a 135 kDa protein in large domestic animals (Okamura et al. 1992); (3) finally, other proteins are released into the epididymal medium, like the angiotensin-convering enzyme (ACE) (Gatti et al. 1999). The study of boar epididymal plasma membrane proteins has resulted in the identification of 32 proteins by mass spectrometry (Belleannée et al. 2011), which have been suggested to control modifications of surface proteins and their correct folding during sperm maturation (TCP-1 complex, H1P1, and HSPs), to participate in sperm-oocyte membrane fusion (VCP with other HSPs) and to mediate the defence of male gametes against oxidative stress (especially from VCP, HSPA2, PRDX5 and GSTM5, which have been described to vary in concentration along the epididymal duct) (Belleannée et al. 2011). Further studies demonstrate that Hsp70 on boar sperm is relocalized and translocated from the inner to the outer leaflet of the sperm plasma membrane as sperm undergo capacitation and acrosome reaction, suggesting an important role of this protein during porcine gamete interaction (Spinaci et al. 2005). Some of the sperm surface proteins identified by Belleannée et al. (2011) have already been reported in the male gamete surface and luminal fluids, such as the angiotensine conversing enzyme (ACE) (Gatti et al. 1999), aldose reductase (AR) (Frenette et al. 2003; Pruneda et al. 2006), arylsulfatase A (ARSA) (Carmona et al. 2002), α-enolase (ENO) (Gitlits et al. 2000), glutathione S-transferase (GST) (Hemachand and Shaha 2003), huntingtin interacting protein 1 (HIP1) (Rao et al. 2001), heat shock 90 and 70 kDa proteins (HSP-90; HSP-70) (Spinaci et al. 2006), α-mannosidase (MAN) (Kuno et al. 2000), lactadherin (MFGE8) (Petrunkina et al. 2003), peroxiredoxin 5 (PRDX5) (Van Gestel et al. 2007), and T-complex protein 1 (TCP1) (Dun et al. 2011). Other identified proteins

have been found to belong to the acrosome (probably released from reacted spermatozoa), such as the acrosine (Puigmulé et al. 2011), LYP4 (Shetty et al. 2003), and sp38 (Mori et al. 1995), or to have cytosolic origins, such as β-tubulin (Pěknicová et al. 2001), valosin-containing protein (VCP) (Geussova et al. 2002), and tyrosine 3-monooxygenase/tryptophan 5-monooxygenase activation protein (YWHAZ; 14-3-3) (Puri et al. 2008), which are known to interact with several membrane proteins.

The knowledge of protein processing during sperm maturation in the epididymal duct could address the question about their role on fertility and their potential use as fertility markers. The fertilin complex (ADAM-1 and ADAM-2) can be mentioned as an example. Fertilin complex expression was first described in guinea pigs (Blobel 2000) and mice (Kim et al. 2006), and a similar pattern was later suggested in bulls (Walker et al. 1996) and more recently in monkeys (Kim et al. 2010) and boars (Fàbrega et al. 2011b). In boars, fertilin maturation involves a regionalized proteolytic processing; most of the 70 kDa testicular ADAM-1 precursors are reduced to the mature 50–55 kDa form when spermatozoa get into the testis-efferent ducts; however, the 70 kDa precursor is not found until the distal corpus. For ADAM-2, a sequential proteolytic cleavage pattern of maturation restricted to proximal caput and corpus has been suggested: the testicular form is processed in the proximal caput into a precursor form of 90 kDa, and then to transient forms of 70–75, 65–70 and 50–55 kDa in the distal caput and corpus, which are further processed in the corpus leading to a final form of 40–43 kDa in the cauda (Fàbrega et al. 2011b). Both, ADAM-1 and ADAM-2 processing may have an essential role in the fertilin complex migration from the whole acrosomal domain to the acrosomal ridge that takes place in sperm at the distal epididymal corpus (resulting in an increase in the local concentration of fertilin that may be crucial for primary sperm-oocyte interactions) (Jones et al. 2007; Van Gestel et al. 2007; Fàbrega et al. 2011b).

Other important plasma membrane proteins present in mature spermatozoa are the GLUT family. This protein family allows the transport of glucose, fructose and related hexoses and pentose through the lipidic bilayer of the spermatozoon, necessary for the uptake of energy sources to maintain basic cell activity as well as specific functions such as motility and fertilization ability (Bucci et al. 2011). In boar, GLUT 1, 2, 3 and 5 have been described and localized (Bucci et al. 2010), and a clear decrease in GLUT 3 transporters has been observed in cryopreserved spermatozoa, suggesting that the cooling/freezing-associated alterations induce changes in the ability of boar sperm to manage their energy levels, thus altering the overall sperm function after thawing (Sancho et al. 2007; Casas et al. 2010).

Furthermore, 14 sperm-specific membrane proteins (SSMPs) ranging from 7.5 to 66 kDa have been described in boar plasma membrane. The identified SSMPs are immunodominant proteins of the sperm membrane; however, the SSMPs repertoire is probably larger and includes minor sperm membrane components that have not yet been identified. Most of them are glycoproteins with an acidic pI and at least one disulfide bond. They overlay all major regions of the spermatozoon and mediate key molecular events of the fertilization process (Haden et al. 2000).

Sperm plasma membrane contains much less cholesterol and glycolipids in boars than in humans (Mann and Lutwak-Mann 1982) due to the loss of cholesterol during the epididymal transit (Nikolopoulou et al. 1985). In contrast, the boar sperm plasma membrane contains relatively high amounts of plasmalogens and other ether-linked phospholipids and lipids with long, polyunsaturated aliphatic chains (Evans et al. 1980). The boar sperm cholesterol/phospholipids molar ratio is about 0.12; 70 % of sperm membrane lipids are phospholipids, choline being the most abundant followed by steroids (Nikolopoulou et al. 1985). Neutral lipids correspond to 25 % of the sperm plasma membrane lipid content and the remaining 5 % correspond to glycolipids (Mann and Lutwak-Mann 1982). This characteristic lipid composition leads to the formation of jellified lipid phases during cooling (Parks and Lynch 1992), which makes boar sperm highly sensitive to cold-shock (Simpson et al. 1987). There is abundant evidence that when boar spermatozoa are refrigerated or frozen both motility and metabolic activity are irreversibly depressed and the acrosome and plasma membranes disrupted. Cold-shock causes loss of cholesterol from sperm and extenders used during cryopreservation must partially supply it (White 1993) (see Sect. 11.2).

Furthermore, during sperm capacitation the organization of plasma membrane proteins and lipids also changes dramatically, allowing sperm to bind to the zona pellucida and thereafter to acrosome react (Gadella et al. 2008) (see also Chap. 7).

1.5 Conclusion

Bearing in mind the particular cell anatomy of boar spermatozoon reinforces the view that, in principle, the function determines the structure. However, for some features of the spermatozoon misunderstandings about structural–functional relationships still exist because certain functions of some structures have not yet been definitively elucidated. Moreover, what is still scarcely understood is the synergistic and concerted fusion in which a variety of identified sperm membrane proteins interact with one another, leading ultimately to the syngamy of sperm and oocyte. It is expected that recent and future advances in proteomics will aid greatly in determining the correct sequence of molecular events leading to sperm–oocyte adhesion (capacitation, induction of acrosome reaction, and sperm-oocyte plasma membrane fusion). Undoubtedly, the highly specialized spermatozoon represents a considerable intellectual challenge to biologists and researchers in the field of reproduction, and persistent studies of the structure, biochemistry, biophysics and functionality of this unique cell will certainly yield still more stimulating rewards in the future. Apart from their basic scientific interest, the thorough knowledge of the wide variety of morphological forms of spermatozoa occurring in boar ejaculate, and also the progress in determining the composition and modus operandi of the specific molecules present in sperm membrane, can be very helpful for improving the efficiency of animal production by means of the currently available biotechnology procedures.

References

Ardón F, Helms D, Sahin, E, Bollwein H, Töpfer Petersen E, Waberski D (2008) Chromatin-unstable boar spermatozoa have little chance of reaching oocytes in vivo. Reproduction 135:461–470

Arya M, Vanha-Perttula T (1985) Lectin-binding pattern of bull testis and epididymis. J Androl 6:230–242

Austin CR (1995) Evolution of human gametes: spermatozoa. In: Grudzinskas JG, Yovich JL (eds) Gametes: the spermatozoon. Cambridge University Press, Cambridge, pp 1–19

Bains HK, Sehgal S, Bawa SR (1992) Human sperm surface mapping with lectins. Acta Anat 145:207–211

Belleannée C, Belghazi M, Labas V, Teixeira-Gomes A-P, Gatti JL, Dacheux J-L, Dacheux F (2011) Purification and identification of sperm surface proteins and changes during epididymal maturation. Proteomics 11:1952–1964

Blobel CP (2000) Functional processing of fertilin: evidence for a critical role of proteolysis in sperm maturation and activation. Rev Reprod 5:75–83

Boerke A, Dieleman SJ, Gadella BM (2007) A possible role for sperm RNA in early embryo development. Theriogenology 68:147–155

Bonet S (1987) Study of ejaculation of a pig submitted to a high rhythm of services in artificial insemination. Scient Gerund 13:35–40

Bonet S (1990) Immature and aberrant spermatozoa in the ejaculate of sus domesticus. Anim Reprod Sci 22:67–80

Bonet S, Briz M (1991a) Comparison between the conventional method and the simple desiccation method in porcine sperm processing for scanning electron microscopy. J Microsc-Oxford 162:291–294

Bonet S, Briz M (1991b) New data on aberrant spermatozoa in the ejaculate of sus domesticus. Theriogenology 35:725–730

Bonet S, Briz M, Fradera A, Egozcue J (1992) Origin, development and ultrastructure of boar spermatozoa with folded tails and with two tails. Hum Reprod 7:523–528

Bonet S, Briz M, Fradera A (1993) Ultrastructural abnormalities of boar spermatozoa. Theriogenology 40:383–396

Bonet S, Briz M, Fradera A (1994a) Contrastación del esperma de porcino al microscopio electrónico de barrido. In: Tratado de ganado porcino: técnicas de contrastación seminal, vol 21. Editorial Luzán 5, Madrid, pp 21–28

Bonet S, Briz M, Fradera A (1994b) Contrastación del esperma de porcino al microscopio electrónico de transmisión. In: Tratado de ganado porcino: Técnicas de contrastación seminal, vol 21. Editorial Luzán 5, Madrid, pp 31–44

Bonet S, Briz M, Pinart E, Camps R, Fradera A, Casadevall M (1995) Light microscopy characterization of sperm morphology. Microsc Anal 9:29–31

Bonet S, Briz M, Pinart E, Sancho S, Garcia-Gil N, Badia E (2000) Morphology of boar spermatozoa. Institut d'Estudis Catalans, Barcelona

Bonet S, Briz M, Pinart E, Sancho S, García-Gil N, Badia E, Bassols J, Pruneda A, Bussalleu E, Yeste M, Casas I, Carreras A (2006) Análisis de la morfología espermática al microscopio electrónico de barrido y al microscopio electrónico de transmisión. In: Bonet S, Martínez E, Rodríguez-Gil JE, Barrera X (eds) Biotecnología de la reproducción porcina: manual de técnicas de reproducción asistida en porcino. Servicio Publicaciones UdG—Red Temática Nacional Reproducción Porcina, Girona, pp 39–50

Brewis IA, Gadella BM (2010) Sperm surface proteomics: from protein lists to biological function. Mol Hum Reprod 16:68–79

Briz M, Fradera A, Bonet S, Pinart E (1993) Analysis of the seminal characteristics of a boar with impaired fertility. Scient Gerund 19:53–60

Briz M (1994) Microscopical analysis of the ejaculated sperm and the sperm epididymal maturation of sus domesticus. Doctoral Thesis, pp 308. Available via http://www.tdx.cat/handle/10803/7632

Briz M, Bonet S, Pinart E, Egozcue J, Camps R (1995) Comparative study of boar sperm coming from the caput, corpus and cauda regions of the epididymis. J Androl 16:175–188
Briz M, Bonet S, Pinart E, Camps R (1996) Sperm malformations throughout the boar epididymal duct. Anim Reprod Sci 43:221–239
Brown CR, von Glos KI, Jones R (1983) Changes in plasma membrane glycoproteins of rat spermatozoa during maturation in the epididymis. J Cell Biol 96:256–264
Bucci D, Isani G, Spinaci M, Tamanini C, Mari G, Zambelli D, Galeati G (2010) Comparative immunolocalization of GLUTs 1, 2, 3 and 5 in boar, stallion and dog spermatozoa. Reprod Domest Anim 45:315–322
Bucci D, Rodriguez-Gil JE, Vallorani C, Spinaci M, Galeati G, Tamanini C (2011) GLUTs and mammalian sperm metabolism. J Androl 32:348–355
Calvo A, Pastor LM, Bonet S, Pinart E, Ventura M (2000) Characterization of the glycoconjugates of boar testis and epididymis. J Reprod Fertil 120:325–335
Calvo A, Pastor LM, Horn R, Pallares J (1995) Histochemical study of glycoconjugates in the epididymis of the hamster (Mesocricetus auratus). Histochem J 27:670–680
Carmona E, Weerachatyanukul W, Soboloff T, Fluharty AL, White D, Promdee L, Ekker M, Berger T, Buhr M, Tanphaichitr N (2002) Arylsulfatase a is present on the pig sperm surface and is involved in sperm-zona pellucida binding. Dev Biol 247:182–196
Casas I, Sancho S, Ballester J, Briz M, Pinart E, Bussalleu E, Yeste M, Fàbrega A, Rodríguez-Gil JE, Bonet S (2010) The HSP90AA1 sperm content and the prediction of the boar ejaculate freezability. Theriogenology 74:940–950
Cooper TG (2005) Cytoplasmic droplets: the good, the bad or just confusing? Hum Reprod 20:9–11
Cooper TG, Yeung C-H (2003) Acquisition of volume regulatory response of sperm upon maturation in the epididymis and the role of the cytoplasmic droplet. Microsc Res Techn 61:28–38
Cooper NJ, McClean RV, Leigh CM, Breed WG (2001) Glycoconjugates on the surface of epididymal spermatozoa in a marsupial, the brushtail possum, Trichosurus vulpecula. Reproduction 122:165–176
Curry MR, Watson PF (1995) Sperm structure and function. In: Grudzinskas JG, Yovich JL (eds) Gametes: the spermatozoon. Cambridge University Press, Cambridge, pp 45–69
Dacheux JL, Dacheux F, Paquignon M (1989) Changes in sperm surface membrane and luminal protein fluid content during epididymal transit in the boar. Biol Reprod 40:635–651
Desantis S, Ventriglia G, Zizza S, Nicassio M, Valentini L, Di Summa A, Lacalandra GM (2010) Lectin-binding sites on ejaculated stallion sperm during breeding and non-breeding periods. Theriogenology 73:1146–1153
Diekman A (2003) Glycoconjugates in sperm function and gamete interactions: how much sugar does it take to sweet-talk the egg? Cell Mol Life Sci 60:298–308
Dun MD, Smith ND, Baker MA, Lin M, Aitken RJ, Nixon B (2011) The chaperonin containing TCP1 complex (CCT/TRiC) is involved in mediating sperm-oocyte interaction. J Biol Chem 286:36875–36887
Ekhlasi-Hundrieser M, Sinowatz F, De Wilke IG, Waberski D, Töpfer-Petersen E (2002) Expression of spermadhesin genes in porcine male and female reproductive tracts. Mol Reprod Dev 61:32–41
Evans RW, Weaver DE, Clegg ED (1980) Diacyl, alkenyl, and alkyl ether phospholipids in ejaculated, in utero-, and in vitro-incubated porcine spermatozoa. J Lipid Res 21:223–228
Fàbrega A, Puigmule M, Dacheux J-L, Bonet S, Pinart E (2011a) Glycocalyx characterization and glycoprotein expression of *sus domesticus* epididymal sperm surface samples. Reprod Fert Develop (published online, (http://dx.doi.org/10.1071/RD11064)
Fàbrega A, Guyonnet B, Dacheux J-L, Gatti J-L, Puigmule M, Bonet S, Pinart E (2011b) Expression, immunolocalization and processing of fertilins ADAM-1 and ADAM-2 in the boar (sus domesticus) spermatozoa during epididymal maturation. Reprod Biol Endocrin 9:96–109
Fazeli A, Hage WJ, Cheng FP, Voorhout WF, Marks A, Bevers MM, Colenbrander B (1997) Acrosome-intact boar spermatozoa initiate binding to the homologous zona pellucida in vitro. Biol Reprod 56:430–438

Flesch FM, Gadella BM (2000) Dynamics of the mammalian sperm plasma membrane in the process of fertilization. Biochim biophys acta (BBA)—reviews on. Biomembranes 1469:197–235

Frenette G, Lessard C, Madore E, Fortier MA, Sullivan R (2003) Aldose reductase and macrophage migration inhibitory factor are associated with epididymosomes and spermatozoa in the bovine epididymis. Biol Reprod 69:1586–1592

Gadella BM, Tsai P-S, Boerke A, Brewis IA (2008) Sperm head membrane reorganisation during capacitation. Int J Dev Biol 52:473–480

Gadella BM, Lopes-Cardoso M, van Golde LM, Colenbrander B, Gadella TW Jr (1995) Glycolipid migration from the apical to the equatorial subdomains of the sperm head plasma membrane precedes the acrosome reaction. Evidence for a primary capacitation event on boar spermatozoa. J Cell Sci 108:935–946

Gatti J-L, Druart X, Guerin Y, Dacheux F, Dacheux J-L (1999) A 105- to 94-kilodalton protein in the epididymal fluids of domestic mammals is angiotensin I-converting enzyme (ACE); evidence that sperm are the source of this ACE. Biol Reprod 60:937–945

Geussova G, Kalab P, Peknicova J (2002) Valosine containing protein is a substrate of cAMP—activated boar sperm tyrosine kinase. Mol Reprod Dev 63:366–375

Gitlits V, Toh B, Loveland K, Sentry J (2000) The glycolytic enzyme enolase is present in sperm tail and displays nucleotide-dependent association with microtubules. Eur J Cell Biol 79:104–111

Gonzalez-Urdiales R, Tejerina F, Domínguez JC, Alegre B, Ferreras A, Pelaez J, Bernal S, Cárdenas S (2006) Técnicas de análisis rutinario de la calidad espermática: motilidad, vitalidad, concentración, resistencia osmótica y morfología espermática. In Manual de Técnicas de Reproducción Asistida en Porcino, pp 19–38

Gupta GS (2005) Sperm maturation in epididymis. In: Proteomics of spermatogenesis. Springer, New York, pp 811–837

Haden NP, Hickox JR, Scott Whisnant C, Hardy DM (2000) Systematic characterization of sperm-specific membrane proteins in swine. Biol Reprod 63:1839–1847

Hammerstedt RH, Hay SR, Amann RP (1982) Modification of ram sperm membranes during epididymal transit. Biol Reprod 27:745–754

Harayama H, Watanabe S, Masuda H, Kanan Y, Miyake M, Kato S (1998) Lectin-binding characteristics of extracts from epididymal boar spermatozoa. J Reprod Dev 44:21–27

Harayama H, Miyake M, Kato S (1999) Immunolocalization of anti-agglutinin for spermatozoa in boars. Mol Reprod Dev 52:269–276

Hemachand T, Shaha C (2003) Functional role of sperm surface glutathione S-transferases and extracellular glutathione in the haploid spermatozoa under oxidative stress. FEBS Lett 538:14–18

Holt WV, Hernandez M, Warrell L, Satake N (2010) The long and the short of sperm selection in vitro and in vivo: swim-up techniques select for the longer and faster swimming mammalian sperm. J Evol Biol 23:598–608

Jiménez I, González-Márquez H, Ortiz R, Betancourt M, Herrera J, Fierro R (2002) Expression of lectin receptors on the membrane surface of sperm of fertile and subfertile boars by flow cytometry. Arch Androl 48:159–166

Jiménez I, González-Márquez H, Ortiz R, Herrera JA, García A, Betancourt M, Fierro R (2003) Changes in the distribution of lectin receptors during capacitation and acrosome reaction in boar spermatozoa. Theriogenology 59:1171–1180

Jonáková V, Manásková P, Kraus M, Liberda J, Tichá M (2000) Sperm surface proteins in mammalian fertilization. Mol Reprod Dev 56:275–277

Jones R, James PS, Howes L, Bruckbauer A, Klenerman D (2007) Supramolecular organization of the sperm plasma membrane during maturation and capacitation. Asian J Androl 9:438–444

Jones R, James PS, Oxley D, Coadwell J, Suzuki-Toyota F, Howes EA (2008) The equatorial subsegment in mamamlian spermatozoa is enriched in tyrosine phosphorylated proteins. Biol Reprod 79:421–431

Jury JA, Frayne J, Hall L (1997) The human fertilin alpha gene is non-functional: implications for its proposed role in fertilization. Biochem J 321:577–581

Kallajoki M, Malmi R, Virtanen I, Suominen J (1985) Glycoconjugates of human sperm surface. A study with fluorescent lectin conjugates and lens culinaris agglutinin affinity chromatography. Cell Biol Int Rep 9:151–164

Kim E, Lee JW, Baek DC, Lee SR, Kim MS, Kim SH, Kim CS, Ryoo Z-Y, Kang HS, Chang KT (2010) Processing and subcellular localization of ADAM2 in the Macaca fascicularis testis and sperm. Anim Reprod Sci 117:155–159

Kim E, Yamashita M, Nakanishi T, Park KE, Kimura M, Kashiwabara SI, Baba T (2006) Mouse sperm lacking ADAM1b/ADAM2 fertilin can fuse with the egg plasma membrane and effect fertilization. J Biol Chem 281:5634–5639

Kirchhoff C, Hale G (1996) Cell-to-cell transfer of glycosylphosphatidylinositol-anchored membrane proteins during sperm maturation. Mol Hum Reprod 2:177–184

Kuno M, Yonezawa N, Amari S, Hayashi M, Ono Y, Kiss L, Sonohara K, Nakano M (2000) The presence of a glycosyl phosphatidylinositol-anchored α-mannosidase in boar sperm. IUBMB Life 49:485–489

Lis H, Sharon N (1998) Lectins: carbohydrate-specific proteins that mediate cellular recognition. Chem Rev 98:637–674

Liu HW, Wang JJ, Chao CF, Muller C (1991) Identification of two maturation-related, wheat-germ-lectin-binding proteins on the surface of mouse sperm. Acta Anat (Basel) 142:165–170

López ML, Grez P, Gribbel I, Bustos-Obregón E (1989) Cytochemical and ultrastructural characteristics of the stallion epididymis (Equus caballus). J Submicrosc Cytol Pathol 21:103–120

Magargee SF, Kunze E, Hammerstedt RH (1988) Changes in lectin-binding features of ram sperm surfaces associated with epididymal maturation and ejaculation. Biol Reprod 38:667–685

Manásková P, Peknicová J, Elzeinová F, Tichá M, Jonáková V (2007) Origin, localization and binding abilities of boar DQH sperm surface protein tested by specific monoclonal antibodies. J Reprod Immun 74:103–113

Mann T, Lutwak-Mann TC (1982) Male reproductive function and semen. Andrologia 14:76

Martin RS (1982) Reproducción e inseminación artificial porcina. Aedos, Barcelona

McLaughlin EA, Frayne J, Barker HL, Jury JA, Jones R, Ford WC, Hall L (1997) Cloning and sequence analysis of rat fertilin alpha and beta-developmental expression, processing and immunolocalization. Mol Hum Reprod 3:801–809

Mori E, Kashiwabara S, Baba T, Inagaki Y, Mori T (1995) Amino acid sequences of porcine Sp38 and proacrosin required for binding to the zona pellucida. Dev Biol 168:575–583

Navaneetham D, Sivashanmugam P, Rajalakshmi M (1996) Changes in binding of lectins to epididymal, ejaculated, and capacitated spermatozoa of the rhesus monkey. Anat Rec 245:500–508

Nicolson GL, Usui N, Yanagimachi R, Yanagimachi H, Smith JR (1977) Lectin-binding sites on the plasma membranes of rabbit spermatozoa: changes in surface receptors during epididymal maturation and after ejaculation. J Cell Biol 74:950–962

Nikolopoulou M, Soucek DA, Vary JC (1985) Changes in the lipid content of boar sperm plasma membranes during epididymal maturation. Biochim Biophys Acta 815:486–498

Nimtz M, Grabenhorst E, Conradt HS, Sanz L, Calvete J (1999) Structural characterization of the oligosaccharide chains of native and crystallized boar seminal plasma spermadhesin PSP-I and PSP-II glycoforms. Eur J Biochem 265:703–718

Okamura N, Dacheux F, Venien A, Onoe S, Huet JC, Dacheux JL (1992) Localization of a maturation-dependent epididymal sperm surface antigen recognized by a monoclonal antibody raised against a 135-kilodalton protein in porcine epididymal fluid. Biol Reprod 47:1040–1052

Overstreet JW, Lin Y, Yudin AI, Meyers SA, Primakoff P, Myles DG, Katz DF, Vandevoort CA (1995) Location of the PH-20 protein on acrosome-intact and acrosome-reacted spermatozoa of cynomolgus macaques. Biol Reprod 52:105–114

Parks JE, Lynch DV (1992) Lipid composition and thermotropic phase behavior of boar, bull, stallion, and rooster sperm membranes. Cryobiology 29:255–266

Pěknicová J, Kubátová A, Sulimenko V, Dráberová E, Viklický V, Hozák P, Dráber P (2001) Differential subcellular distribution of tubulin epitopes in boar spermatozoa: recognition of class III Î²-tubulin epitope in sperm tail. Biol Reprod 65:672–679

Pelaez J, Long JA (2007) Characterizing the glycocalyx of poultry spermatozoa: I. Identification and distribution of carbohydrate residues using flow cytometry and epifluorescence microscopy. J Androl 28:342–352

Peterson R, Chaudhry P, Tibbs B (1989) Calcium-binding proteins of boar spermatozoan plasma membranes: identification and partial characterization. Gamete Res 23:49–60

Petrunkina AM, Harrison RAP, Töpfer-Petersen E (2000) Only low levels of spermadhesin AWN are detectable on the surface of live ejaculated boar spermatozoa. Reprod Fert Develop 12:361–371

Petrunkina AM, Gehlhaar R, Drommer W, Waberski D, Töpfer-Petersen E (2001) Selective sperm binding to pig oviductal epithelium in vitro. Reproduction 121:889–896

Petrunkina AM, Lakamp A, Gentzel M, Ekhlasi-Hundrieser M, Töpfer-Petersen E (2003) Fate of lactadherin P47 during post-testicular maturation and capacitation of boar spermatozoa. Reproduction 125:377–387

Petruszak JA, Nehme CL, Bartles JR (1991) Endoproteolytic cleavage in the extracellular domain of the integral plasma membrane protein CE9 precedes its redistribution from the posterior to the anterior tail of the rat spermatozoon during epididymal maturation [published erratum appears in J Cell Biol 1991 Nov; 115(3): following 880]. J Cell Biol 114:917–927

Phelps BM, Koppel DE, Primakoff P, Myles DG (1990) Evidence that proteolysis of the surface is an initial step in the mechanism of formation of sperm cell surface domains. J Cell Biol 111:1839–1847

Primakoff P, Hyatt H, Myles DG (1985) A role for the migrating sperm surface antigen PH-20 in guinea pig sperm binding to the egg zona pellucida. J Cell Biol 101:2239–2244

Pruneda A, Pinart E, Bonet S, Yeung C-H, Cooper T (2006) Study of the polyol pathway in the porcine epididymis. Mol Reprod Dev 73:859–865

Pruneda A, Pinart E, Briz M, Sancho S, García-Gil N, Badia E, Kádár E, Bassols J, Bussalleu E, Yeste M, Bonet S (2005) Effects of a high semen-collection frequency on the quality of sperm from ejaculates and from six epididymal regions in boars. Theriogenology 63:2219–2232

Puigmulé M, Fàbrega A, Yeste M, Bonet S, Pinart E (2011) Study of the proacrosin/acrosin system in epididymal, ejaculated and in vitro capacitated boar spermatozoa. Reprod Fert Develop 23:837–845

Puri P, Myers K, Kline D, Vijayaraghavan S (2008) Proteomic analysis of bovine sperm YWHA binding partners identify proteins involved in signaling and metabolism. Biol Reprod 79:1183–1191

Rao DS, Chang JC, Kumar PD, Mizukami I, Smithson GM, Bradley SV, Parlow AF, Ross TS (2001) Huntingtin interacting protein 1 is a clathrin coat binding protein required for differentiation of late spermatogenic progenitors. Mol Cell Biol 21:7796–7806

Sancho S, Casas I, Ekwall H, Saravia F, Rodriguez-Martinez H, Rodriguez-Gil JE, Flores E, Pinart E, Briz M, Garcia-Gil N, Bassols J, Pruneda A, Bussalleu E, Yeste M, Bonet S (2007) Effects of cryopreservation on semen quality and the expression of sperm membrane hexose transporters in the spermatozoa of Iberian pigs. Reproduction 134:111–121

Sanz L, Calvete JJ, Mann K, Schöpfer W, Schmid ER, Töpfer-Petersen E (1991) The amino acid sequence of AQN-3, a carbohydrate-binding protein isolated from boar sperm location of disulphide bridges. FEBS Lett 291:33–36

Schroter S, Osterhoff C, McArdle W, Ivell R (1999) The glycocalyx of the sperm surface. Hum Reprod Update 5:302–313

Shetty J, Wolkowicz MJ, Digilio LC, Klotz KL, Jayes FL, Diekman AB, Westbrook VA, Farris EM, Hao Z, Coonrod SA, Flickinger CJ, Herr JC (2003) SAMP14, a novel acrosomal membrane-associated, glycosylphosphatidylinositol-anchored member of the Ly-6/urokinase-type plasminogen activator receptor superfamily with a role in sperm-egg interaction. J Biol Chem 278:30506–30515

Simpson AM, Swan MA, White IG (1987) Susceptibility of epididymal boar sperm to cold shock and protective action of phosphatidylcholine. Gamete Res 17:355–373

Spinaci M, Volpe S, Bernardini C, De Ambrogi M, Tamanini C, Giovanna Galeati ES (2005) Immunolocalization of heat shock protein 70 (Hsp 70) in boar spermatozoa and its role during fertilization. Mol Reprod Dev 72:534–541

Spinaci M, Volpe S, Bernardini C, de Ambrogi M, Tamanini C, Seren E, Galeati G (2006) Sperm sorting procedure induces a redistribution of Hsp70 but not Hsp60 and Hsp90 in boar spermatozoa. J Androl 27:899–907

Srivastav A (2000) Maturation-dependent glycoproteins containing both N- and O-linked oligosaccharides in epididymal sperm plasma membrane of rhesus monkeys (Macaca mulatta). J Reprod Fertil 119:241–252

Syntin P, Dacheux F, Druart X, Gatti JL, Okamura N, Dacheux JL (1996) Characterization and identification of proteins secreted in the various regions of the adult boar epididymis. Biol Reprod 55:956–974

Taitzoglou IA, Kokoli AN, Killian GJ (2007) Modifications of surface carbohydrates on bovine spermatozoa mediated by oviductal fluid: a flow cytometric study using lectins. Int J Androl 30:108–114

Thaler CD, Cardullo RA (1995) The mammalian sperm surface: molecular and cellular aspects. In: Grudzinskas JG, Yovich JL (eds) Gametes: the spermatozoon. Cambridge University Press, Cambridge, pp 20–44

Töpfer-Petersen E (1999) Carbohydrate-based interactions on the route of a spermatozoon to fertilization. Hum Reprod Update 5:314–329

Töpfer-Petersen E, Ekhlasi-Hundrieser M, Tsolova M (2008) Glycobiology of fertilization in the pig. Int J Dev Biol 52:717–736

Tulsiani DR, Skudlarek MD, Holland MK, Orgebin-Crist MC (1993) Glycosylation of rat sperm plasma membrane during epididymal maturation. Biol Reprod 48:417–428

Van Gestel RA, Brewis IA, Ashton PR, Brouwers JF, Gadella BM (2007) Multiple proteins present in purified porcine sperm apical plasma membranes interact with the zona pellucida of the oocyte. Mol Hum Reprod 13:445–454

Waberski D, Meding S, Dirksen G, Weitze KF, Leiding C, Hahn R (1994) Fertility of long-term-stored boar semen: influence of extender (Androhep and Kiev), storage time and plasma droplets in the semen. Anim Reprod Sci 36:145–151

Wagner A, Ekhlasi-Hundrieser M, Hettel C, Petrunkina A, Waberski D, Nimtz M, Töpfer-Petersen E (2002) Carbohydrate-based interactions of oviductal sperm reservoir formation-studies in the pig. Mol Reprod Dev 61:249–257

Walker JM, Gravel P, Golaz O (1996) Identification of glycoproteins on nitrocellulose membranes using lectin blotting. In: Walker JM (ed) The protein protocols handbook. Humana Press, England, pp 603–617

Waters SI, White JM (1997) Biochemical and molecular characterization of bovine fertilin alpha and beta (ADAM 1 and ADAM 2): a candidate sperm-egg binding/fusion complex. Biol Reprod 56:1245–1254

White IG (1993) Lipids and calcium uptake of sperm in relation to cold shock and preservation: a review. Reprod Fert Develop 5:639–658